Precambrian Research 279 (2016) 103–122

Contents lists available at ScienceDirect

Precambrian Research

journal homepage: www.elsevier.com/locate/precamres

A new ~3.46 Ga asteroid impact ejecta unit at Marble Bar, Pilbara Craton, Western Australia: A petrological, microprobe and laser ablation ICPMS study

Andrew Glikson [a,b,*], Arthur Hickman [c], Noreen J. Evans [d], Christopher L. Kirkland [d,e], Jung-Woo Park [g,h], Robert Rapp [g], Sandra Romano [c,f]

[a] Geoscience Australia, P.O. Box 378, Canberra, A.C.T. 2601, Australia
[b] Planetary Science Institute, Australian National University, Acton, Australian Capital Territory, Australia
[c] Geological Survey of Western Australia, 100 Plain Street, East Perth, W.A. 6004, Australia
[d] Applied Geology, John de Laeter Centre, TIGeR, Curtin University, Bentley, WA 6102, Australia
[e] Centre for Exploration Targeting, Curtin Node, Department of Applied Geology, Western Australian School of Mines, Curtin University, WA 6102, Australia
[f] Centre for Exploration Targeting, School of Earth and Environment, The University of Western Australia, 35 Stirling Highway, Crawley, W.A. 6004, Australia
[g] Research School of Earth Sciences, Australian National University, Acton, Canberra 2601, Australia
[h] School of Earth and Environmental Sciences & Research Institute of Oceanography, Seoul National University, Seoul 151-747, South Korea

ARTICLE INFO

Article history:
Received 5 November 2015
Revised 30 March 2016
Accepted 2 April 2016
Available online 9 April 2016

Keywords:
Impact
Spherules
Archean
Geochemistry
Pilbara
Marble Bar

ABSTRACT

The Archean rock record contains seventeen asteroid impact ejecta units that represent the terrestrial vestiges of an extended late heavy bombardment (LHB). Correlated impact ejecta units include 3472–3470 Ma impact spherule layers in the Barberton Greenstone Belt, Kaapvaal Craton, South Africa, and the Pilbara Craton, Western Australia, and several ejecta units dated between 3250 and 3220 Ma and between 2630 and 2480 Ma (Lowe and Byerly, 2010; Lowe et al., 2003, 2014). This paper reports the discovery and investigation of a new impact ejecta unit within the Marble Bar Chert Member (MBCM) of the felsic volcanic Duffer Formation, east Pilbara Craton, Western Australia. The age of the MBCM is constrained by a 3459 ± 2 Ma U–Pb zircon date from the uppermost volcanic unit of the Duffer Formation and by a 3449 ± 3 Ma U–Pb zircon date from the overlying felsic volcanic Panorama Formation, stratigraphically above the intervening un-dated Apex Basalt. The ejecta unit, observed in a drill core (ABDP 1) ~4 km south-southwest of Marble Bar, consists of multiple lenses and bands of almost totally silicified impact spherules 1–2 mm in diameter. All internal primary textures of the spherules have been destroyed. Nonetheless, Fe-rich spherule rims, largely composed of secondary siderite, are well preserved. Chemical analyses of the rims reveal iron-magnesium carbonate displaying high Fe, Mg, Ni, Co and Zn. Whole-rock and in-situ analyses (X-ray fluorescence, Inductively Coupled Plasma Mass Spectrometry (ICPMS), electron-microprobe (EMP) and EMP-calibrated laser ICPMS) reveal that the rims contain high Ni abundances and high Ni/Cr ratios (<50). The spherules are separated by an arenite matrix and spherule lenses also occur within bedded chert. The spherules are particularly visible over some ~14 m of true stratigraphic thickness in which chert breccia is interpreted to represent a tsunami-generated diamictite affected by hydrothermal fragmentation and veining. Despite the almost total silicification of the MBCM whole-rock analysis by NIS Fire Assay and ICPMS indicates high Ir (2 ppb) and a low Pd/Ir ratio (2.0), consistent with geochemical features of impact ejecta units. Dense concentrations of spherules at the 57–58 m level and the 77 m level of the core, separated by banded chert, raise the possibility of two distinct impact events. Stratigraphic and isotopic age data distinguish between the 3459 and 3449 Ma age of the MBCM ejecta unit and ~3470.1 ± 1.9 Ma impact ejecta units in the Antarctic Creek Member, Mount Ada Basalt, about 40 km to the west of Marble Bar. In combination with a 3472 ± 2.3 Ma impact unit in the Barberton greenstone belt, these impact ejecta units record large Paleoarchean asteroid impacts, significant for understanding early bombardment rates on Earth and early crustal evolution.

* Corresponding author at: Geoscience Australia, P.O. Box 378, Canberra, A.C.T. 2601, Australia.

http://dx.doi.org/10.1016/j.precamres.2016.04.003
0301-9268/

1. Introduction

The identification of 17 Archean asteroid impact ejecta units, some of which may be correlated, up to 3.47 Ga in the Barberton Greenstone Belt, Kaapvaal Craton, South Africa, and the Pilbara region of Western Australia, including clusters spanning 3.25–3.22 Ga and 2.63–2.48 Ga, may represent terrestrial vestiges of an extended late heavy bombardment (LHB) (Lowe and Byerly, 2010; Lowe et al., 2003, 2014). Major asteroid impacts likely had an effect on early crustal evolution (Jones et al., 2003), a documented example being the abrupt shift from mafic–ultramafic volcanism to clastic sedimentary basins in the Barberton and Pilbara between ~3.25 and 3.22 Ga, an interval associated with a cluster of large asteroids (Glikson and Vickers, 2005, 2010). The Pilbara region of northwestern Western Australia is known to contain evidence for asteroid impacts dated as 3.47 Ga, 2.63 Ga, 2.57 Ga, 2.56 Ga and 2.48 Ga (Lowe and Byerly, 1986; Lowe et al., 1989; Simonson and Glass, 2004; Glikson, 2004; Glikson and Vickers, 2010).

This paper reports the identification of 1–2 mm-diameter silica-dominated spherules in the 3459–3449 Ma Marble Bar Chert Member (MBCM) of the Duffer Formation (Warrawoona Group) (Figs. 1 and 2). The spherules were first observed by us (AG and AH) in 2014 in the diamond drill core of ABDP 1 hole drilled in 2003 as part of the Archean Biosphere Drilling Project (Fig. 3). This core provides a complete 110 m-thick (corrected true thickness) stratigraphic section through the MBCM drilled 4 km south-southwest of Marble Bar (Figs. 1–3). Previous studies of the core did not report any spherules (Suganuma et al., 2006; Hoashi et al., 2009; Kato et al., 2009; Li et al., 2013). The spherules occur in layers of bedded chert and are dispersed in quartz-dominated arenite and in the siliceous matrix of fragmented chert. Rare spherules are also sporadically preserved within massive gray chert interpreted to be in part of intrusive hydrothermal origin and in part silicified *in situ* chert. Spherules occur in discrete layers only in the lower 14 m of the MBCM, a true stratigraphic thickness which may represent the reworking and redeposition of a primary impact fallout deposit.

Principal criteria for recognition of asteroid impact ejecta units include ~1–2 mm scale spherules commonly displaying well defined rims, inward-radiating quench textures of K-feldspar or chlorite, a centrally offset bubble, trace Ni-rich phases such as Ni-chromite, trace metal (Ni, Co, Cr), PGE and $^{53}Cr/^{52}Cr$ anomalies (Glass and Burns, 1988; Kyte et al., 1992, 2003; Shukolyukov et al., 2000; Simonson and Glass, 2004). Impact effects in oceans and shallow seas include generation of tsunami deposits and excavation of the sea floor and this assists with their identification in the field. In terms of these criteria, it is important to note that the almost total silicification of the MBCM (generally > 90% SiO_2) has destroyed the primary internal textures of the spherules. However spherule rims are well preserved.

To date, two impact ejecta layer occurrences in the age range of ~3474–3468 Ma have been documented, one in the Barberton region of South Africa (Lowe et al., 2003; Lowe and Byerly, 2010) and one 40 km west of Marble Bar at North Pole dome (Lowe and Byerly, 1986; Byerly et al., 2002; Glikson et al., 2004). To test the possibility that the MBCM spherules may also be of an impact origin two separate concentrations of spherules were studied in detail, one from 57.1 m and another from 58.1 m in the core. Core samples were studied by optical petrology, SEM–EDS analysis, XRD diffraction, whole-rock XRF and ICPMS geochemistry, LA-ICPMS and EMP micro-analysis.

2. Marble Bar Chert Member (MBCM) and ABDP 1 core

The Marble Bar Chert member (MBCM) forms the uppermost part of the felsic volcanic Duffer Formation in the Marble Bar greenstone belt of lower greenschist facies (Figs. 1 and 2). The Duffer Formation is a component of the Warrawoona Group which is the oldest of three groups making up the 3530–3235 Ma Pilbara Supergroup (Hickman, 2012; Hickman and Van Kranendonk, 2012). Type section exposures of the MBCM along the Coongan River include spectacular variegated red and white banded chert and have been the subject of numerous previous studies (Kjellgren, 1976; DiMarco and Lowe, 1989; Sugitani, 1992; Minami et al., 1995; Kojima et al., 1998; Van Kranendonk et al., 2001; Kato and Nakamura, 2003; Orberger et al., 2006; Suganuma et al., 2006; Van Kranendonk, 2006; van den Boorn et al., 2007, 2010; Hoashi et al., 2009; Olivier et al., 2012; Li et al., 2013; Rasmussen et al., 2014). The Duffer Formation (Fig. 2) is almost entirely composed of felsic volcanic rocks, making U–Pb zircon age determination relatively easy. Dating of these volcanic rocks, in both the Marble Bar and the adjacent Coongan greenstone belts (Appendix A), constrains the depositional age of the Duffer Formation to between 3474 and 3459 Ma. The youngest published date, from close to the top of Duffer Formation, 3459 ± 2 Ma (De Vries et al., 2006), constrains the maximum depositional age of the MBCM. Lacking felsic volcanic rocks the overlying Apex Basalt has not been directly dated. However, felsic volcanic rocks of the overlying Panorama Formation were dated in the Marble Bar greenstone belt. Ages (Appendix A, Fig. 1 of Appendix A), include 3446 ± 5 Ma (JW95-001, de Vries et al., 2006) and 3449 ± 3 Ma (GSWA 94770, Thorpe et al., 1990, 1992). Both samples contained older zircon inherited from the underlying Duffer Formation. Elsewhere in the east Pilbara the maximum depositional age of the Panorama Formation is 3448 ± 6 Ma (Wingate et al., 2012). It is concluded that the combined age range of the MBCM and the overlying Apex Basalt is 3459–3449 Ma. A substantial part of this interval probably accounted for deposition of the MBCM because plume-related basaltic formations were erupted quickly.

In the type area at Marble Bar Pool, 3 km west–southwest from the town of Marble Bar, the MBCM is approximately 60 m thick and is steeply overturned, dipping 80° east–northeast but with stratigraphic way-up to the west–southwest. At the ABDP 1 drilling site, located 3 km southeast of Marble Bar Pool (Hickman, 2005), the MBCM is overturned and was drilled from its stratigraphic base upwards (Hoashi et al., 2009).

The MBCM was deposited above the >5 km-thick felsic volcanic succession of the Duffer Formation which in the Marble Bar and several other greenstone belts is a volumetrically important component of the 3530–3426 Ma Warrawoona Group. The Warrawoona Group is the oldest group of the 15–20 km-thick Pilbara Supergroup and consists of a predominantly mafic volcanic succession composed of a series of volcanic cycles (Figs. 1 and 2). At higher stratigraphic levels the Pilbara Supergroup contains a series of erosional unconformities overlain by conglomerate and sandstone (Buick et al., 1995; Hickman, 2012). Clastic sediments deposited upon these unconformities include detrital zircons between 3676 and 3550 Ma (Kemp et al., 2015), indicating uplift and erosion of older granitic crust underlying or bordering the Pilbara Supergroup. Rare outcrops of 3660–3580 Ma gneiss are exposed within the Paleoarchean granites and granite gneisses that form 30–100 km diameter domes in the east Pilbara (Hickman, 2012).

The MBCM extends over ~10,000 km^2 and has been identified in five greenstone belts in the east Pilbara Craton (Fig. 1). Although historically referred to as a "chert", the MBCM is now known to be mainly composed of silicified fine-grained clastic sediments and tuffaceous material which, as shown by their fine lamination, were deposited in low-energy environments (DiMarco and Lowe, 1989; Orberger et al., 2006; Hoashi et al., 2009). The thickness of the MBCM is variable along strike ranging from 50 to 200 m over 30 km in the Marble Bar area (Hoashi et al., 2009). About

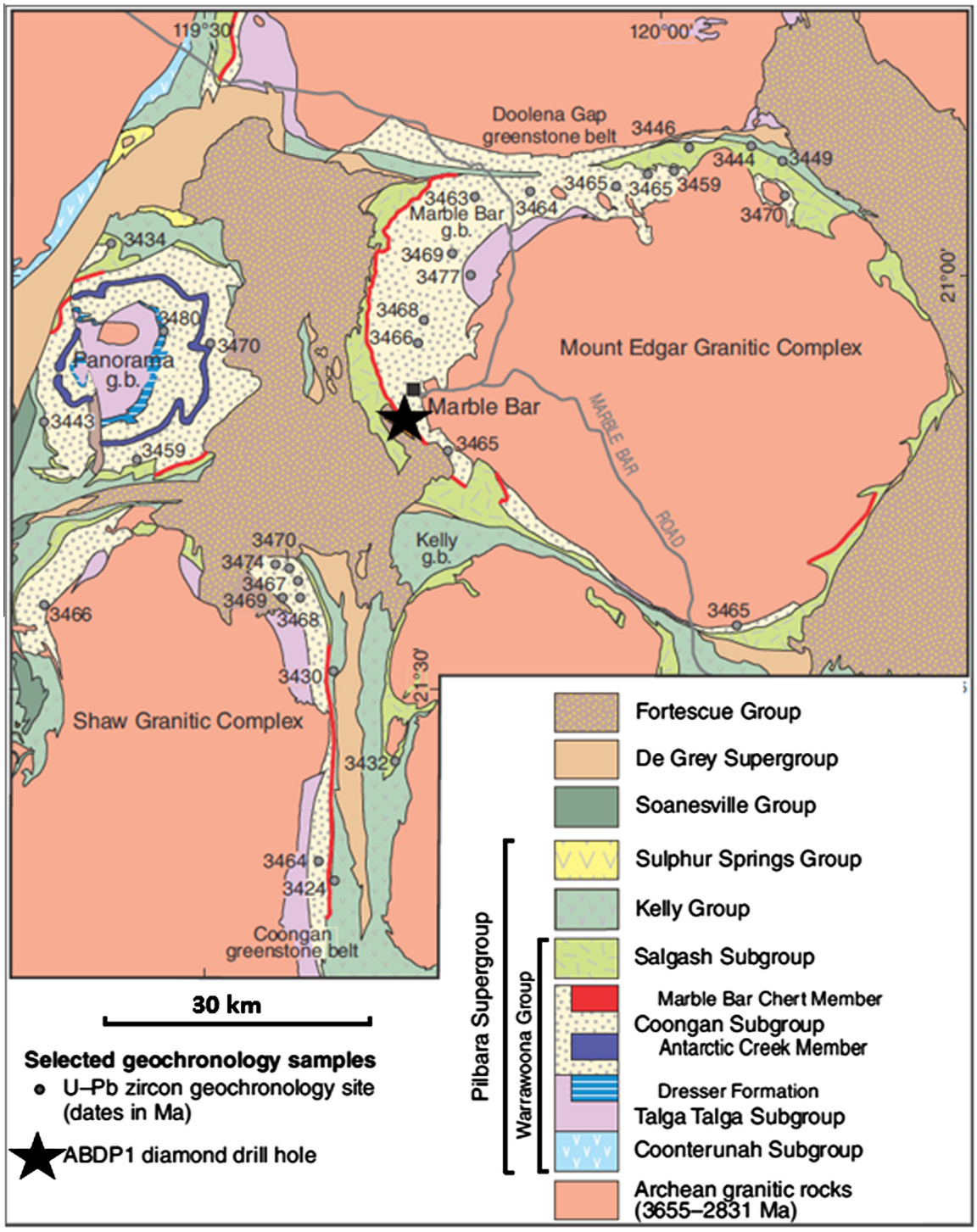

Fig. 1. Geological map of the eastern part of the Pilbara Craton, showing the main stratigraphic groups and subgroups and key geochronological ages. For further isotopic age evidence refer to Appendix A.

500 m north of Marble Bar Pool, Kato and Nakamura (2003) measured a 45 m section whereas at the Marble Bar pool itself Oliver and Cawood (2001) recorded the thickness as 60 m. Some 3 km southeast of the pool, at the ABDP 1 drilling site, the true stratigraphic thickness is 110 m. These differences arise mainly from intrusion of cross cutting dolerite sills and subvolcanic feeders of the overlying Apex Basalt into the base of the MBCM. In some instances the dolerite breaks through the MBCM to merge into the overlying Apex Basalt (Van Kranendonk et al., 2001).

A range of depositional settings has been proposed for the MBCM, including mid-oceanic ridge, basin plain, island arc, continental margin, volcanic caldera, and lacustrine. Uniformitarian comparisons with oceanic settings (Kimura et al., 1991; Isozaki et al., 1991; Kitajima et al., 2001; Komiya et al., 2002; Kato and Nakamura, 2003; Terabayashi et al., 2003) are precluded by the extensive occurrence of felsic volcanic units and evidence for earlier granitic crust in the east Pilbara region (Green et al., 2000; Van Kranendonk et al., 2002, 2007; Hickman, 2008, 2012; Kemp et al., 2015).

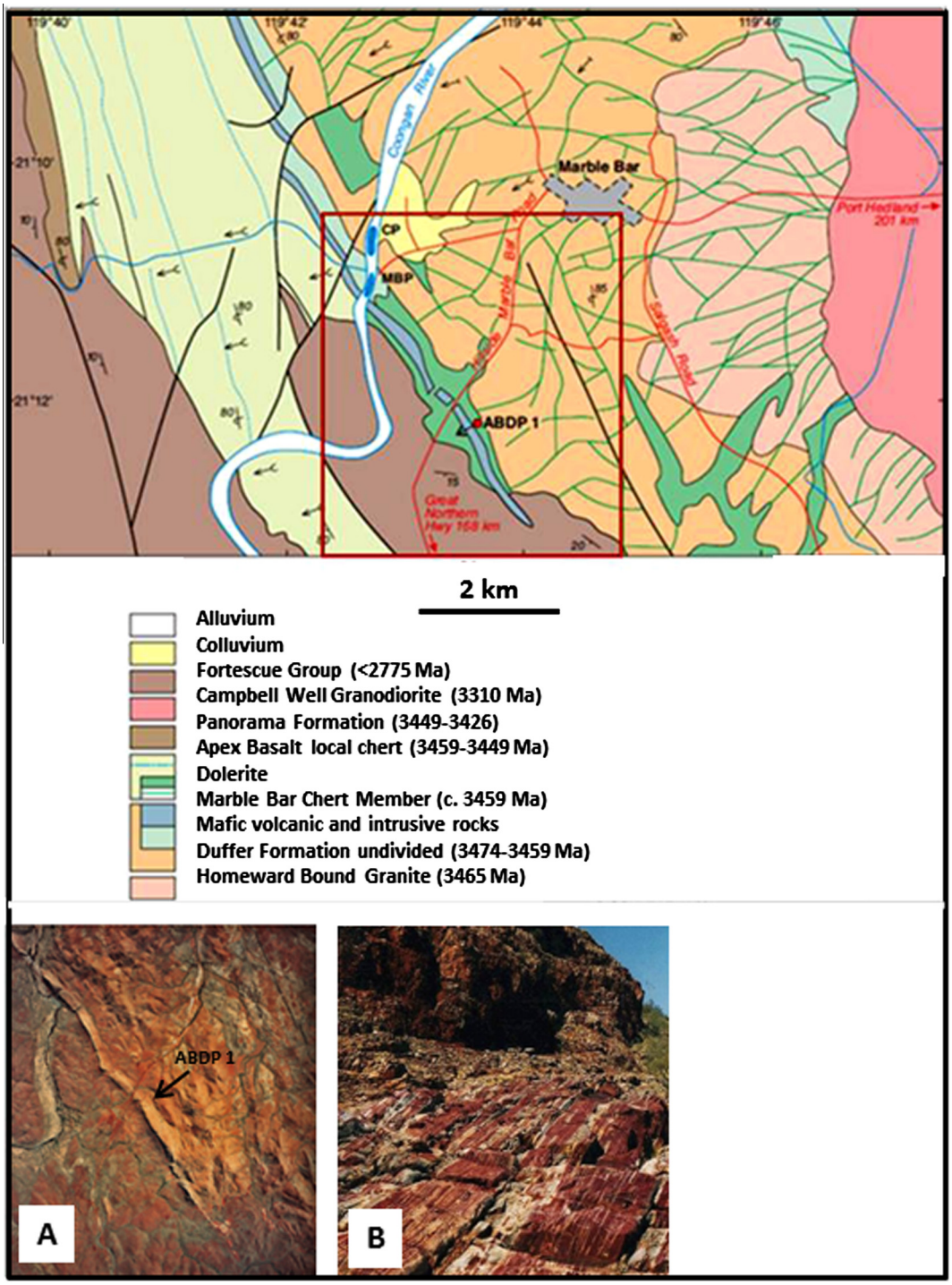

Fig. 2. Geological sketch map and aerial photograph of the Marble Bar area, eastern Pilbara Craton, showing the Marble Bar Chert Member. Insert (A) aerial photograph – location indicated with red square on the map. Insert (B) banded red and white chert of the Marble Bar Chert Member in Coongan River south and west of Marble Bar town. Location indicated on the map. MBP – Marble Bar Pool; CP – Chinaman Pool. (For interpretation of the references to colour in this figure legend, the reader is referred to the web version of this article.)

It has been suggested that the Pilbara Supergroup was deposited as a volcanic plateau overlying continental sialic crust (Van Kranendonk et al., 2007, 2014; Hickman, 2012). Alternatively Glikson (2014) proposed deposition in volcanic rift zones located within older granitoid terrains. DiMarco and Lowe (1989) interpreted the MBCM, previously termed Towers Formation, to have been deposited in shallow water on a regionally extensive erosional surface, above the volcanic and volcaniclastic sedimentary rocks now assigned to the Duffer Formation. Although the Duffer Formation was eroded prior to deposition of the MBCM, an unconformity has not been identified.

The MBCM at Marble Bar Pool and in the ABDP 1 core contains a significant amount of transgressive dark gray chert containing numerous angular blocks of the banded chert. Oliver and Cawood (2001) documented rock pavements at Marble Bar Pool, which display blocks of banded chert up to 10 m across within a matrix of

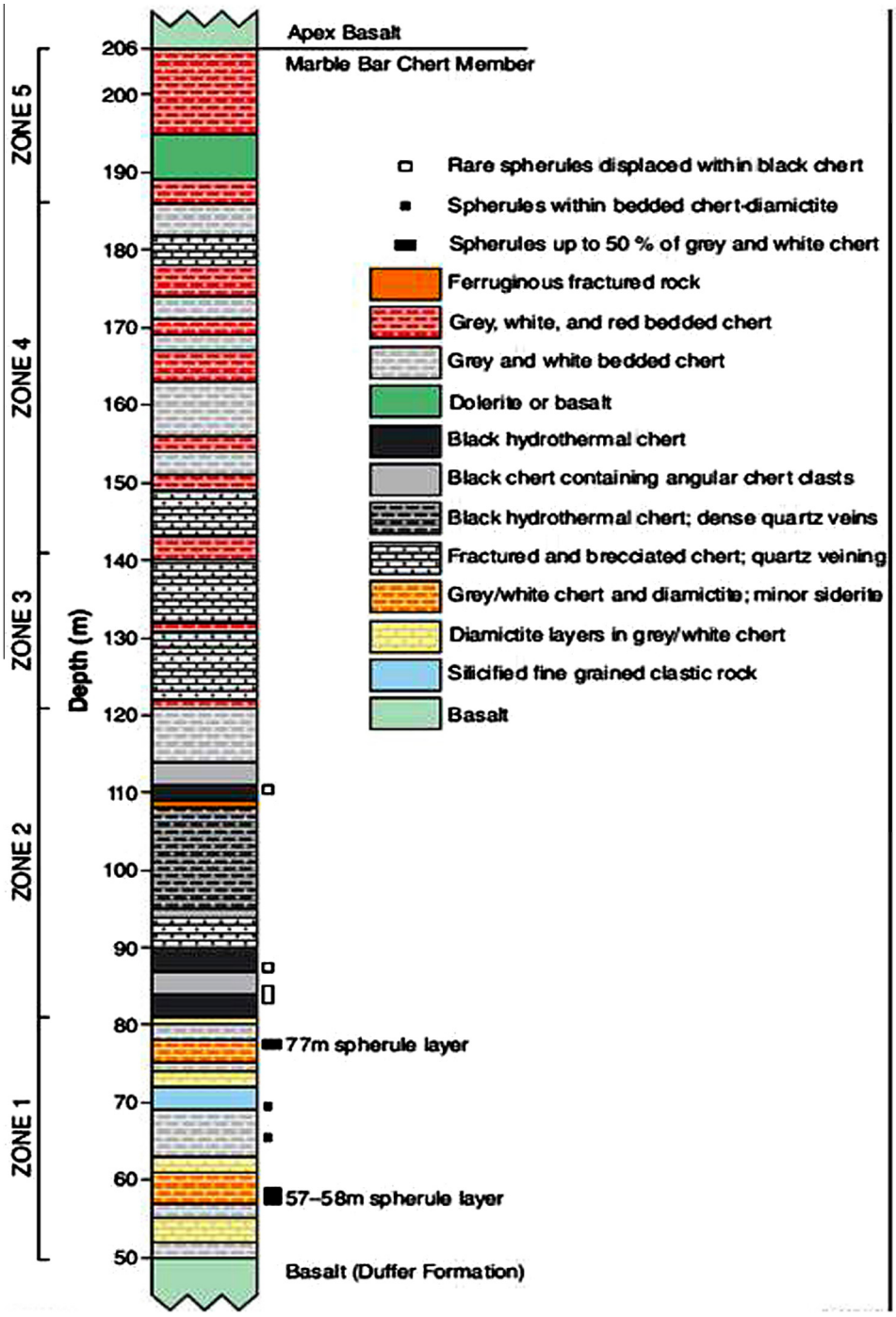

Fig. 3. Part of the lithological drill-hole section of the ABDP 1 drill hole (21.20439 S; 119.72718 E), showing the spherule-bearing diamictite intervals in Zones 1 and 2.

dark gray chert containing chert fragments down to <1 mm across. Chert forms discordant veins along faults and lateral injection along bedding, likely associated with siliceous hydrothermal fluids. Silicification of the MBCM occurred during or shortly after deposition of the clastic sediments and is attributed to hydrothermal activity, either during waning volcanic activity of the Duffer Formation, or as a hydrothermal prelude to mafic volcanism of the next volcanic cycle. The local presence of coarse clastic sedimentary rocks in the MBCM has been attributed to high-density turbidity currents and mass transport complexes (Olivier et al., 2012).

3. Spherules within the ABDP 1 core

Spherules found in the ABDP 1 drill core are located within the depth range of 57–110 m (Fig. 3). The MBCM in the ABDP 1 core has an apparent thickness of 156 m and, a true thickness of approximately 110 m, and within the core has been divided by Hoashi et al. (2009) into five zones, which from the bottom to the top are (Fig. 3):

Zone 1. Sulfide-bearing gray-white chert overlying basalt of the Duffer Formation

Zone 2. Black hydrothermal chert containing chert clasts

Zone 3. Brecciated chert and red-white banded chert

Zone 4. Alternating red and white banded chert

Zone 5. Gray-white and red-white chert intercalated with dolerite and basalt.

Zones 2 and 3 contain dark gray hydrothermal chert with breccia and quartz veining. Thus, widely scattered spherules in the interval between 82 and 110 m may have been dislodged and transported from Zone 1 by hydrothermal activity. The gray chert in Zone 2 is a hydrothermal deposit in large veins and blocks of chert which have been moved from other levels of the stratigraphy. Likewise the spherules must have been transported. Some spherules occur within a silicified clastic deposit containing matrix-supported partly rounded fragments of banded chert plates (Fig. 4). Partial rounding of clasts (Fig. 4) and the lack of dark gray hydrothermal chert in spherule-bearing sections of Zone 1 indicate that these coarse clastic units are sedimentary and composed of transported material. Olivier et al. (2012) reported basaltic and granitic clasts near Marble Bar Pool. However within the MBCM in Zone 1 of the ABDP 1 core clasts consist exclusively of chert, suggesting the diamictite was derived from currents that disrupted the sea floor within the MBCM basin.

The distinction between *in situ* spherule layers and re-deposited spherules is not clear. Well-rounded to oblate spherules, mostly up to 1 mm (Fig. 5) and in some instances above 1 mm in diameter (Fig. 6), comprise internal zones of microcrystalline quartz mosaics rimmed by clouded cryptocrystalline siderite and quartz (Figs. 6A–D, 8). Some spherule rims consist of two layers of siderite separated by a layer of quartz (Fig. 8). This may be due to growth by accretion processes or possibly to late-stage silica invasion of the siderite in the rims. Rare angular banded particles are present in the spherule layers. These are similar to flow-banded particles in the Carawine spherule-bearing breccia that Simonson et al. (2005) compared with Muong-Nong type tektites (Fig. 6E and F) and similar fragments associated with microkrystite spherules in the JIL, DGS4 and SMB impact ejecta units (Glikson, 2004). Broken and quartz-injected spherules are rare (Fig. 6G and H). Spherules may be agglutinated (Fig. 5) and are separated by a mostly cryptocrystalline clouded matrix consisting of quartz accompanied by trace K-feldspar, siderite, pyrite and arsenopyrite. SEM backscatter images indicate concentration of siderite grains at the spherule rims (Fig. 7), high Fe at the rims and less commonly in internal zones, and high Si in internal sectors of the spherules (Fig. 8).

4. Petrography, whole rock and mineral chemistry

Lithological summaries of ABDP 1 core samples containing spherules are given in Table 1. Core samples were collected from 11 intervals within the depth range 57.1–110.3 m, measured from base to top (Table 1; Fig. 3) and 2 samples, at 57.1 m and at 58.1 m, were subjected to detailed analyses. This included examination of half cores (Fig. 4), polished slabs (Fig. 5) and polarizing microscopy using 0.03 mm thin sections (Fig. 6). Mineral identifications were conducted by X-ray Diffraction (XRD) and scanning Electron Microscopy (SEM) coupled with Energy Dispersive Spectrometry (EDS) (Fig. 7). Whole rock geochemical analyses were

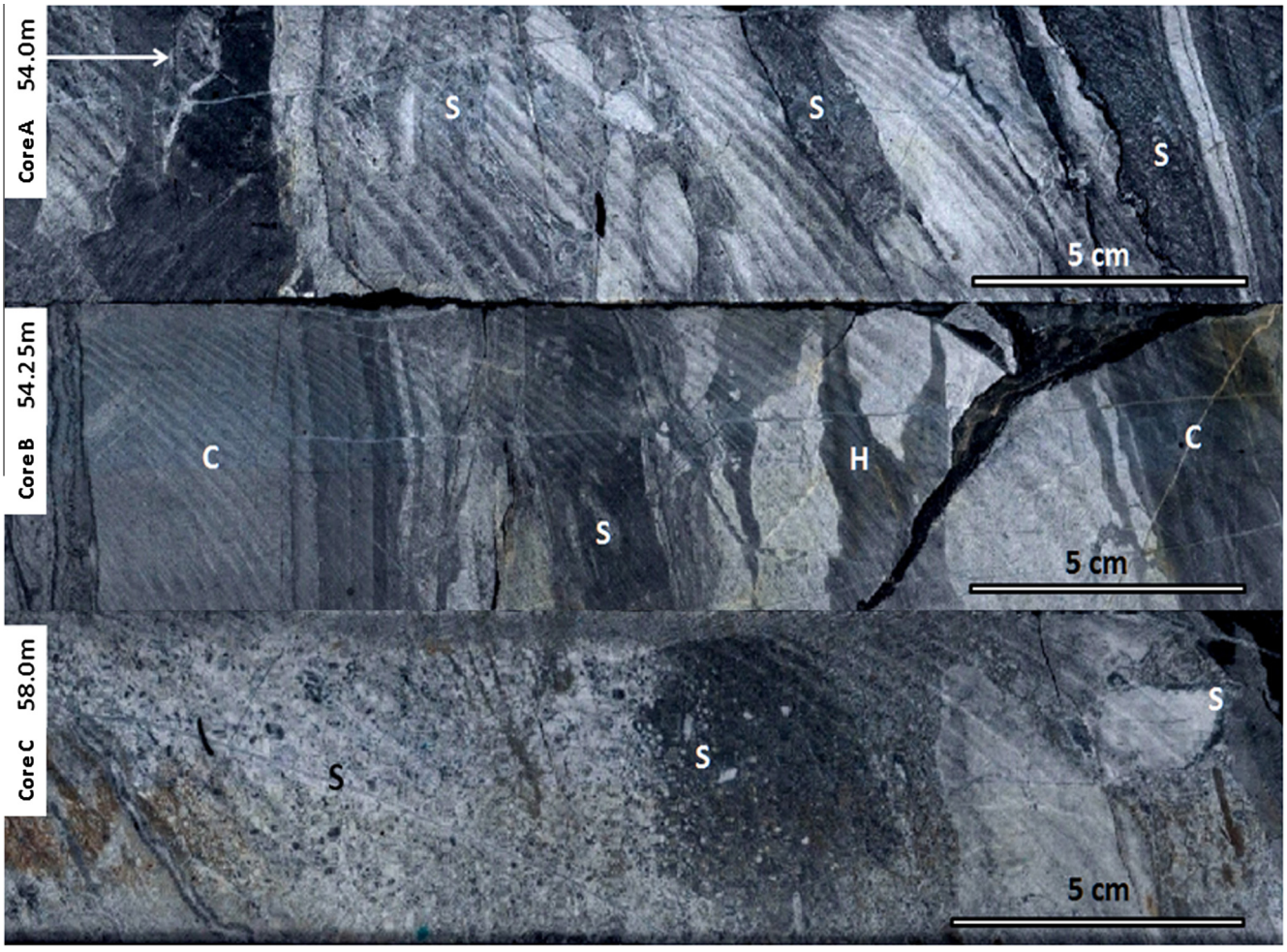

Fig. 4. Spherule-bearing chert diamictite intervals of the ABDP 1 drill hole Zone 1. S – spherule-bearing matrix; C – chert fragments; M – matrix; H – hydrothermally altered matrix.

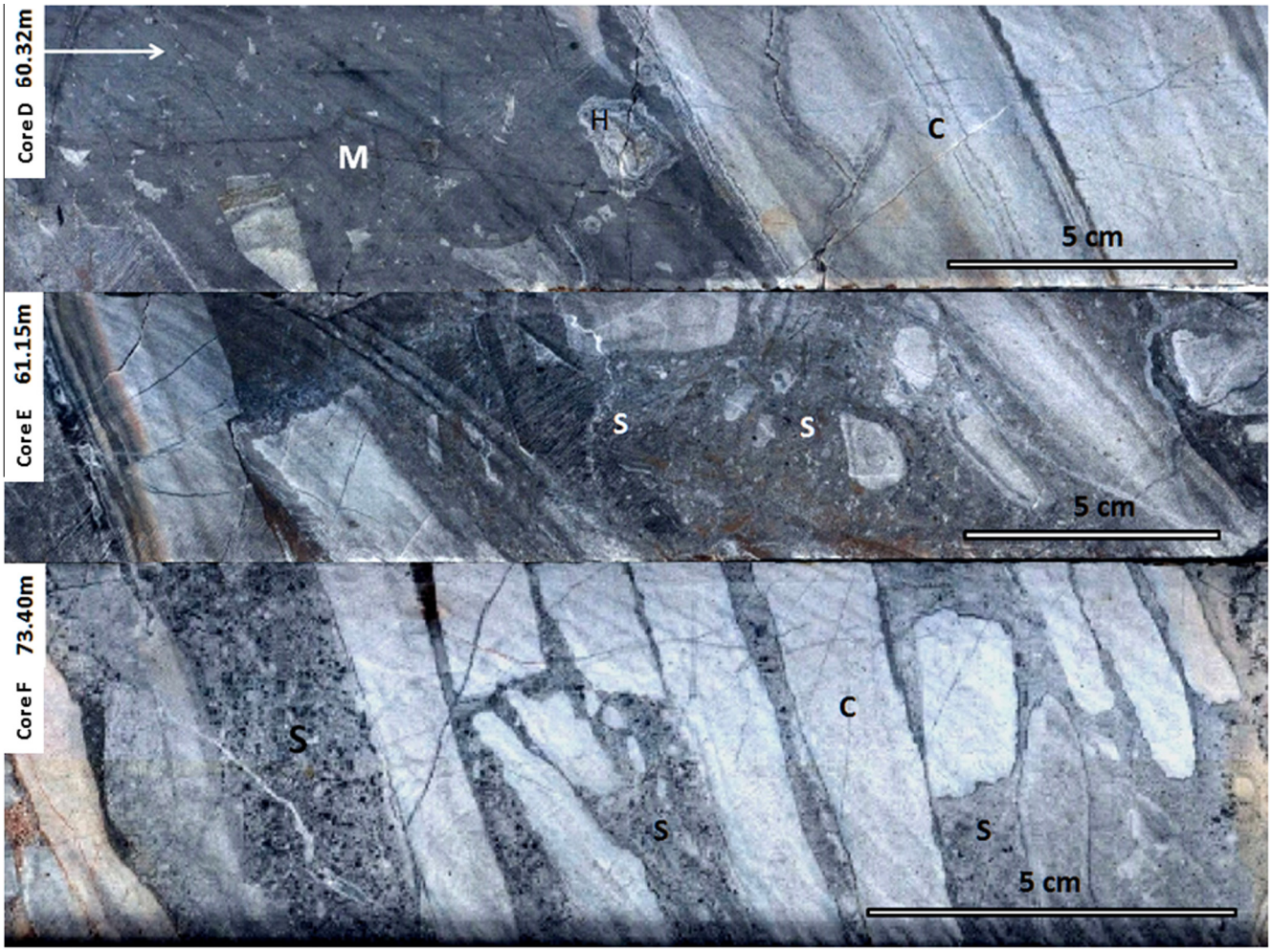

Fig. 4 (*continued*)

conducted by X-ray fluorescence (XRF) and whole-rock inductively coupled plasma mass spectrometry (ICP-MS). Micro-geochemical analyses were conducted by LA-ICPMS and Electron Microprobe (EMP). Investigations of internal spherule compositional variations were performed by (A) LA-ICPMS count mapping (RSES and Curtin University laboratories); (B) EMP element mapping (Centre for Exploration Technology, The University of Western Australia); (C) EMP-calibrated LA-ICPMS analyses (RSES and Curtin University laboratories); (D) EMP-calibrated LA-ICPMS mineral analyses (RSES laboratory).

5. Analytical methods

5.1. X-ray diffraction

Whole rock X-ray mineral analyses were conducted using a Bruker D4 X-ray Diffractometer (XRD) at angles of 5° to 70° 2θ, in 0.020° steps at 1 s per step, using a Cu anode X-ray tube. Minerals were identified using Bruker Diffracplus software. Bruker Topas V3 was used to quantify minerals.

5.2. SEM/EDS (Scanning Electron Microscopy and Energy Dispersive Spectrometry)

The analyses used the JEOL Jed-2300 Analysis Station at acceleration voltage 15.0 kV; probe current 1.0 nA; live time 150 s; energy range 0–20 keV.

5.3. Whole rock XRF

Whole rock analyses of a spherule-bearing rock sample of about 100 g from core level 57.1 m were conducted at Geoscience Australia (GA) in Canberra and from core sample 58.1 m by Intertek Genalysis (Table 2), using a sample of ~100 g. The GA laboratory sample was jaw crushed and sub-samples (50–70 g) ground in a tungsten carbide ring mill. Major and minor elements (Si, Ti, Al, Fe, Mn, Mg, Ca, Na, K, P and S) were determined by wavelength-dispersive XRF on fused disks (Norrish and Hutton, 1969). Precision is estimated as better than ±1% of the reported values. The elements As, Ba, Cr, Cu, Ni, Sc, V, Zn & Zr were determined by pressed pellet on a wavelength dispersive XRF (Norrish and Chappell (1977). The trace elements Cs, Ga, Nb, Pb, Rb, Sb, Sn, Sr, Ta, Th, U, Y and the rare earth elements (REE) were analyzed on an Agilent 7500 ICPMS with a reaction cell (Eggins et al., 1997) on solutions obtained by dissolution of fused glass disks (Pyke, 2000). Analytical precision was ±5% to ±10% at low levels (<20 ppm). The agreement between XRF and ICP-MS is within 10%. Loss on Ignition (LOI) was obtained by gravimetry after combustion at 1100 °C. FeO abundances were determined by digestion and electrochemical titration using a modified methodology based on Shapiro and Brannock (1962).

A 100 g sample of 1/4 core from 58.1 m (Table 2) was analyzed by Intertek Genalysis, Perth, and was pulverized in an agate mill to avoid contamination by Cr, W, and Co. Elemental analysis of Ag, As, Ba, Be, Bi, Cd, Cd, Co, Cs, Dy, Er, Eu, Ga, Ge, Gd, Ho, In, La, Li, Lu, Mo, Nb, Nd, Pb, Pr, Rb. Re, Sb, Se, Sm, Sn, Sr, Ta, Tb, Te, Th, Tl, Tm, U, W,

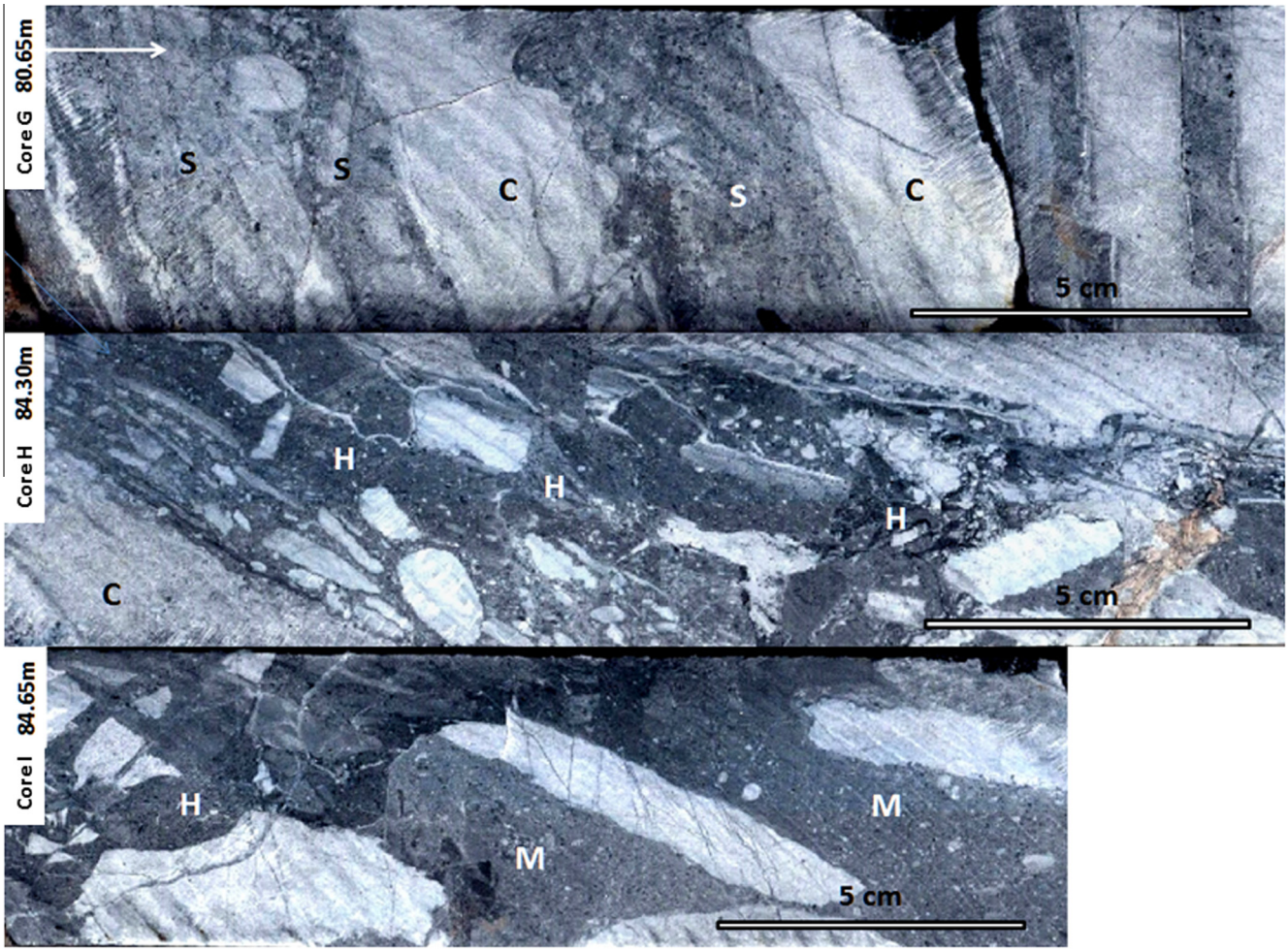

Fig. 4 (*continued*)

Y, and Yb was undertaken by ICPMS following multi-acid digest, including hydrofluoric, nitric, perchloric, and hydrochloric acids in Teflon beakers. Al, Ca, Cr, Cu, Fe, K, Mg, Mn, Na, Ni, P, S, Sc, Ti, V, and Zn were analyzed by Inductively Coupled Plasma Optical (Atomic) Emission Spectrometry (ICP OES) after multi-acid digest, including hydrofluoric, nitric, perchloric, and hydrochloric acids in Teflon tubes. Percentage concentrations of Co, Fe, and Ni were analyzed by Flame Atomic Absorption Spectrometry (AAS) following multi-acid digest, including hydrofluoric, nitric, perchloric, and hydrochloric acids.

The elements Au, Ir, Os, Pd, Pt, Rh, and Ru were analyzed by Inductively Coupled Plasma Mass Spectrometry following Fire Assay Nickel Sulfide Collection. Standards used were AMIS0278, AMIS0013, OREAS 24b, OREAS 45d, OREAS 77a, MPL-5, and WMS-1a, along with two control blanks and an acid blank. Detection limits for the NiS-fire assay collection ICPMS method were Au, 2 ppb; Ir, 1 ppb; Os, 1 ppb; Pd, 1 ppb; Pt, 1 ppb; Re, 2 ppb; Rh, 1 ppb; Ru, 1 ppb. The absolute concentration errors (in ppb) for the PGE elements depend on the concentration levels (ppb) determined (sample at 58.1 m), as reported by Genalyis: Ir ± 0.27 (at 2 ppb); Pd ± 0.82 (at 4 ppb); Pt ± 1.65 (at 6 ppb); Rh ± 0.23 (at 1 ppb); Ru ± 0.55 (at 6 ppb); and Os ± 0.34 (at 3 ppb). For Au, the standard uncertainty was ±1.14 (at 5 ppb), and for Re it was ±1.4 (at 5 ppb).

5.4. Electron Microprobe Analysis (EMP)

EMP analysis was performed at two facilities. The procedure used in each is outlined below. Major-element compositions of the constituent minerals (siderite and quartz) of the spherules were determined by EMP using wavelength-dispersive spectrometry with the Cameca SX-100 electron microprobe in the Research School of Earth Sciences at ANU (Appendix B) and the University of Western Australia (Appendix D).

The Cameca SX-100 was operated at an accelerating voltage of 15 kV, an electron beam current of 20 nA, and a beam diameter of approximately 1 μm. Counting times on the K-alpha X-ray peaks for major-elements (Mg, Al, Si, Ca, Fe) were 10–20 s, and 30 s for minor-elements and alkalis (e.g., Ti, Mn, Na and K); background count rates measured on either side of the peak for one-half the peak counting-time. Calibrations were made on simple oxides (e.g., MgO, Al_2O_3, SiO_2, TiO_2), and synthetic ($CaSiO_3$) or natural silicate mineral standards (rhodonite, albite, sanidine, olivine). In addition to spot analyses of individual mineral grains within the spherulitic bodies, broad-beam EMP analysis along the length of the LA-ablation ICP-MS traverses across the spherules were also carried out using a 100 μm diameter, defocused electron beam, providing an estimate of the average "bulk" composition of the spherules.

The calibration of LA-ICPMS analyses by EMP analyses of spherule rims and interiors allows quantitative determination of the abundance of trace metal (Appendices B–F). Individual points to calibrate the LA-ICPMS work, and semi-quantitative element maps were produced at the Centre of Microscopy, Characterization and Analysis, The University of Western Australia on the JEOL 8530F microprobe. Measuring conditions were 20 kV acceleration voltage and 40 nA beam current. Counting times for Ca, Fe and Mn were

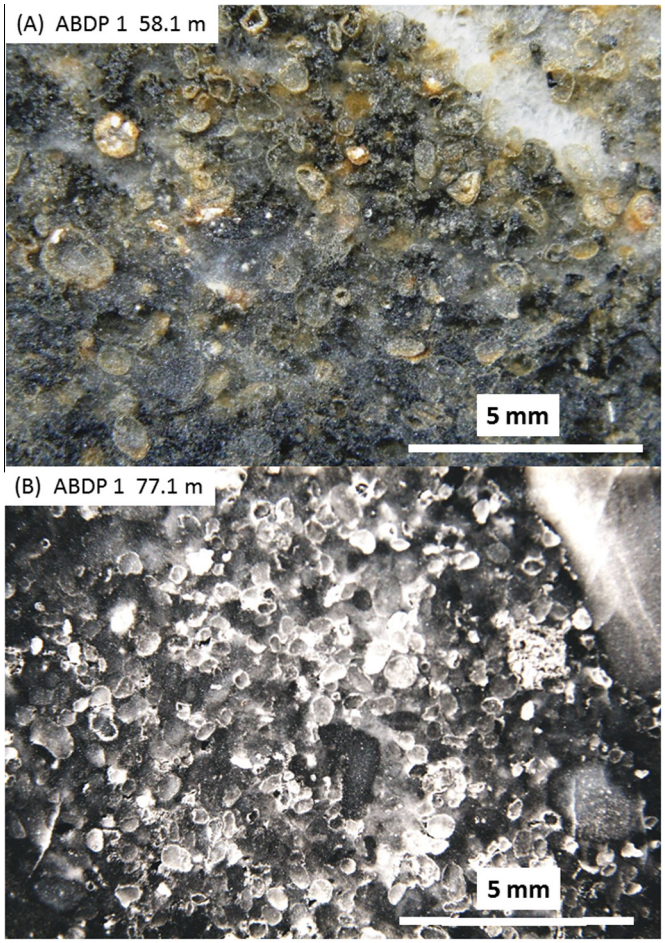

Fig. 5. Macro-photographs of MBCM rock slabs displaying densely packed spherules. (A) Rounded to sub-rounded spherules bordering a black chert unit and cut by a quartz vein; (B) rounded to sub-rounded spherules bordering on white chert.

20 s, K, Si, Mg, Na and Al (30 s), S for 50 s, Ni, Cr, V, and Ti for 70 s, and Co for 100 s. Used standards were orthoclase (Si, K), rutile (Ti), corundum (Al), Cr2O3 (Cr), Magnetite (Fe), Cobalt (Co), V, Ni and Mn glass, periclase (Mg), Durango apatite (Ca), jadeite (Na) and barite (S). For the quantitative microanalysis a Mean Atomic Number (MAN) background correction was used. The semi-quantitative maps were measured on following spectrometers: S (PETJ), Mg (TAP), Cr (LiFH), Mn (LiF), Ti (LiF); Ca (PETJ), Si (TAP), Ni (LiFH), Fe (LiF) and V (LiF).

5.5. Trace element mapping and spot analysis by LA-ICPMS

LA-ICPMS analyses were undertaken in two laboratories. The procedure for each is detailed below. LA-ICPMS analysis of trace elements in polished samples was undertaken at the GeoHistory Facility, John de Laeter Centre, Curtin University utilizing a Resonetics Resolution M-50A-LR incorporating a Compex 102 excimer LA, coupled to an Agilent 7700 s quadrupole ICP-MS. Following a 20 s period of background analysis, samples were spot ablated for 30 s at a 7 Hz repetition rate, using a 50 μm beam and LA energy (measured at the sample surface) of 2.5 J cm^{-2}. Oxide polyatomic interferences were minimized by tuning mass spectrometer settings to a ThO/Th ratio of <0.5% on NIST 610. The sample cell was flushed with ultrahigh purity He (0.68 L min^{-1}) and N_2 (2.8 mL min^{-1}) and high purity Ar was employed as the plasma carrier gas. For Fe-rich phases, international glass standard GSD-1G was used as the primary reference material, to calculate elemental concentrations using Fe (mass 57) determined by Electron Microprobe (EMP) as the internal standard element and to correct for instrument drift on all elements except PGE + Au. Certified sulfide standard Laflamme Po726 (synthetic pyrrhotite doped with platinum group elements and Au) was utilized as the primary standard for calculation of Au content.

PGE anomalies were detected above the level of detection limit of 0.1–0.01 ppm, where the detection limit depends on the particular element and each concentration level. Many of the PGE concentration levels presented in Appendix F are considered to be significant. Future work may focus on more precise measurement of PGE levels in the Marble Bar Chert Member spherules.

For silicate-rich phases, NIST-610 was the primary reference material using LA-ICPMS determined ^{29}Si for internal standardization and drift correction. Standard blocks were run every 20 unknowns. The mass spectra were reduced using Iolite (Paton et al., 2011 and references therein). Data were collected on a total of 31 elements (^{107}Ag, ^{75}As, ^{197}Au, ^{137}Ba, ^{209}Bi, ^{59}Co, ^{52}Cr, ^{63}Cu, ^{193}Ir, ^{24}Mg, ^{55}Mn, ^{95}Mo, ^{60}Ni, ^{189}Os, ^{208}Pb, ^{105}Pd, ^{195}Pt, ^{101}Ru, ^{103}Rh, ^{34}S, ^{121}Sb, ^{77}Se, ^{28}Si, ^{29}Si, ^{118}Sn, ^{47}Ti, ^{205}Tl, ^{51}V, ^{66}Zn and ^{90}Zr).

Trace element concentrations of quartz-rich spherule center and siderite-rich spherule rim were also analyzed by LA-ICPMS at the Research School of Earth Science, Australian National University using a Lambda Physik COMPex 110 excimer LA (λ = 193 nm), ANU-designed HelEx ablation cell, and an Agilent 7700 ICP-MS. The cross-section analyses were performed using spot size of 105 μm, a LA pulse rate of 5 Hz and scan rate of 1 or 5 μm per second. NIST-610 glass (Jochum et al., 2011) was used as the primary standard for trace elements. ^{29}Si and ^{57}Fe were used for correcting yield differences between unknown samples and the NIST standard for quartz-rich spherule interior parts and siderite, respectively. Data reduction was performed using the Iolite software package (Paton et al., 2011). The isotopes used to determine the concentrations are as follows: ^{24}Mg, ^{27}Al, ^{29}Si, ^{45}Sc, ^{49}Ti, ^{51}V, ^{53}Cr, ^{55}Mn, ^{57}Fe, ^{59}Co, ^{61}Ni, ^{63}Cu, ^{66}Zn, ^{155}Gd, ^{179}Hf. The compositions of the quartz-rich spherule interior matrix were calculated by assuming that the quartz-rich matrix contains Si contents of 46.7 wt% (stoichiometric Si contents in quartz). The Ti, V, Cr, Co, Ni, Cu and Zn concentrations of the siderite were quantified using average Fe contents of 38.0 wt % measured by EMP with assumption that the signals of these elements were only produced by siderite. The minimum time duration of the signal segments used for the calculation was 10 s.

6. Results

Apart from SiO_2, which can form up to 99% of the rock, the spherules include variable amounts of siderite and Fe-oxide and minor amounts of K-feldspar, sulfide, arsenic and lead-bearing particles and clay-alteration in the cores of sulfide grains. The results of SEM–EDS indicate spherule rims are marked by grains of magnesian and iron-rich phase (Fe = ~46–51%; Mg = ~2.0–5.0%) (Table 2), identified by EMP analyses as siderite (Appendix B).

A milled whole rock sample from depth 57.8 m contains quartz (66.1%), muscovite (19.1%), kaolinite (10.8%) and vermiculite (3.9%). SEM–EDS analyses indicate abundance of quartz and of siderite. Geochemical analyses of spherules using multiple methods (whole rock XRF and ICPMS, SEM–EDS, Ni sulfide fire essay ICPMS, EMP and LA-ICPMS) at different laboratories all gave high Ni and Ir contents for a rock with >93% SiO_2, and high Ni/Cr ratios and Pd/Ir ratios of ~2.0 (Table 2).

6.1. LA-ICPMS elemental mapping, transects, EMP-calibrated point and mineral analysis of spherules

EMP mapping of spherules displays well-defined Fe-rich and Si-poor rims whereas internal sectors are Si-rich except in local

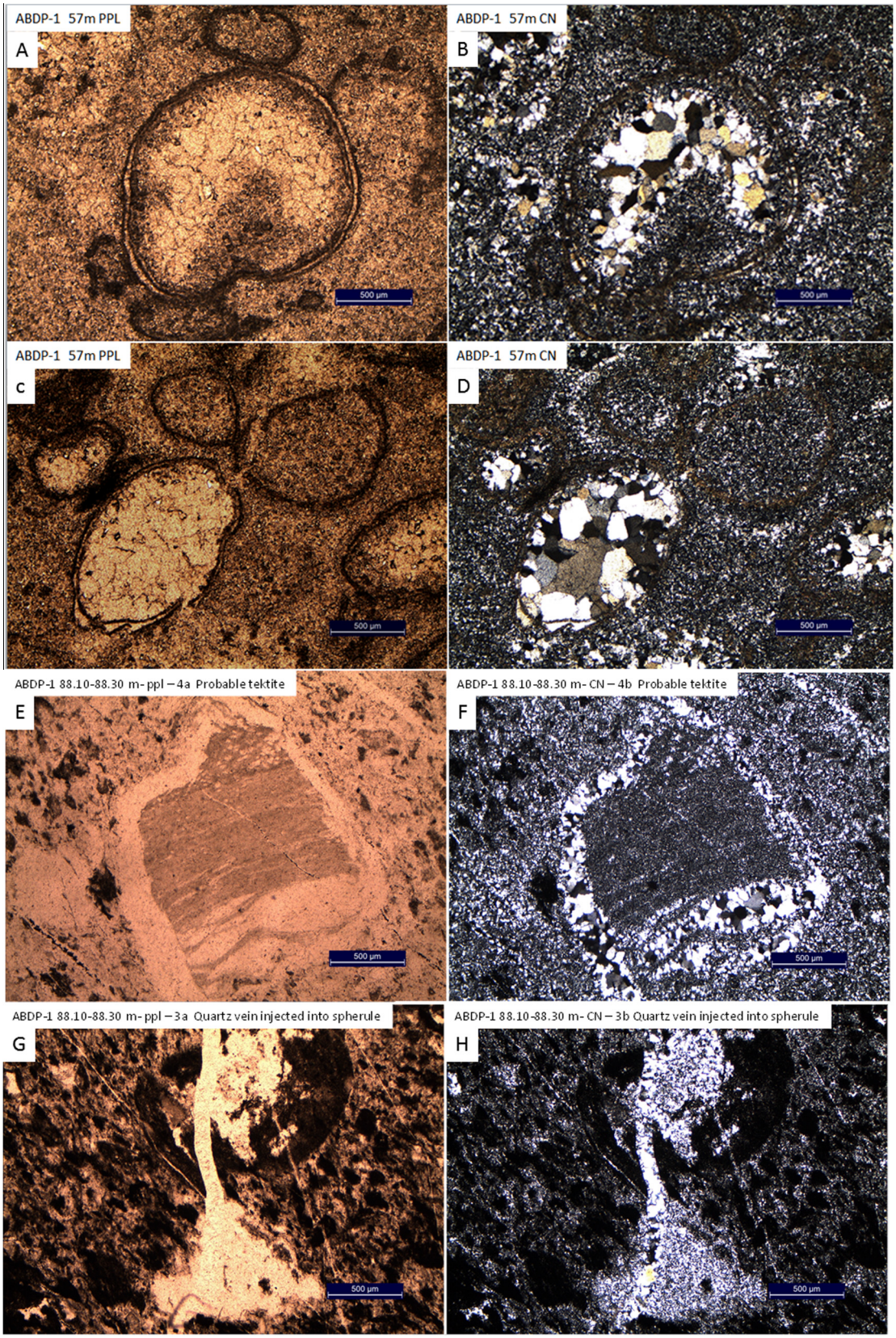

Fig. 6. Polarizing microcopy images of spherule-bearing sample from ABDP 1 drill hole, showing (A–D) well-formed spherules consisting of quartz mosaics and dark siderite-rich rims. (E and F) flow banded fragment mantled by quartz, similar to tektite fragments of the Spherule Marker Bed and Carawine breccia (Simonson et al., 2004). (G and H) Broken spherule injected by quartz vein.

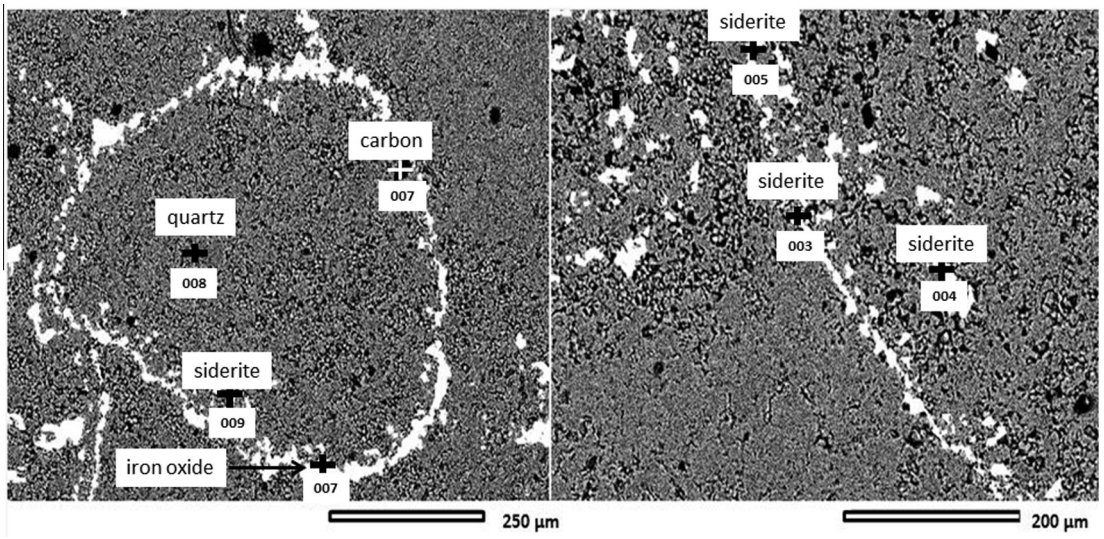

Fig. 7. Sample 57.1 m. SEM images of spherules defined by siderite-rich rims. Analyst: D. DiBugnara. The bright grains are mostly siderite.

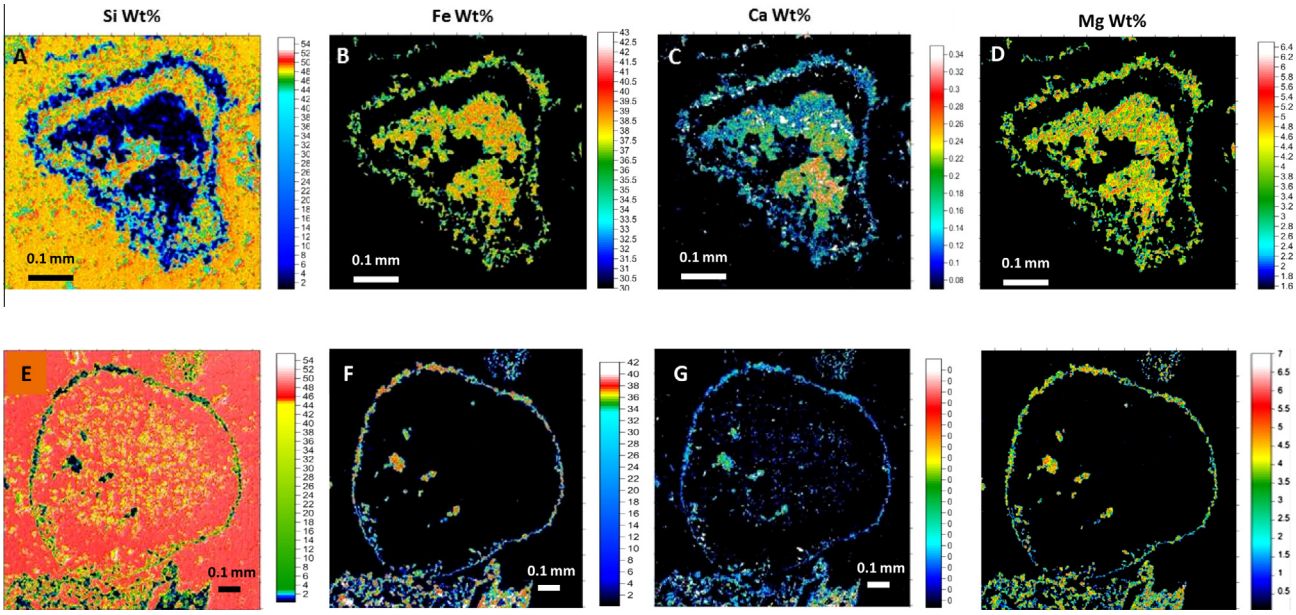

Fig. 8. EMP semi-quantitative mapping for 2 spherules in sample 58.1 for Si, Fe, Ca and Mg, displaying siderite-rich rims and quartz-dominated interiors.

concentrate ions of siderite (Fig. 8). LA-ICPMS analyses of trace elements in siderite are presented in Table 3. LA-ICPMS count mapping displays high counts of Ni and Cr at spherule rims (Fig. 9A and B), high Co (Fig. 9D) and Zn (Fig. 9G) and lower Si (Fig. 9E). Internal sectors are mostly Si-rich and Fe-poor (Fig. 8). Some sections through spherules were cut close to spherule margins, chiefly within the siderite-rich rims, and these sections give the appearance of siderite extending into the central parts of spherules. Low-Ni zones in the rims of some spherules (Fig. 9A) are due to the presence of almost pure quartz between layers of siderite, possibly representing late-stage invasion of quartz into central sections of siderite rims.

A continuous LA-ICPMS transect through spherules and matrix (Fig. 10) displays positive anomalies in V/Si, Co/Si, Cr/Si and Ni/Si at points A, B and C due to enrichment of metals and depletion of Si at the rim of the spherules. By contrast a quartz-rich spherule interior between points B and C displays low metal concentrations (Fig. 10b). Calibration of chosen sections along a LA-ICP-MS traverse (Fig. 10) using average siderite composition obtained by EMP analysis allows determination of the abundances of Ni, Cr and Co and their ratios (Fig. 10; Appendices B and C), yielding high trace metal values and high Ni/Cr ratios in spherule rims. These values contrast with average komatiites (Ni/Cr ~ 0.24–0.76) (Fiorentini et al., 2011) and basalts (Ni/Cr ~ 0.17–0.9) (Fig. 11) (Appendix G).

Detailed analyses of spherules by EMP-calibrated LA-ICPMS micro-analyses along the rims and across individual spherules (Fig. 12) indicate FeO values in spherule rims up to <55%, Ni values up to 219 ppm and Ni/Cr ratios up to 51.

LA-ICPMS spot analyses (Appendices C, E, F) (Supplementary data) give average compositions of heterogeneous mixtures that in most analyses vary with ablation depth. Analyses along cross-sections of spherules likewise indicate high Ni values (<59 ppm) and high Ni/Cr ratios (<8.9) at the rims and, in rare instances, in

Table 1
Spherule-bearing diamictite core samples collected from drill core ABDP 1 (21.20439 S, 119.72718 E) (drilled from stratigraphic bottom to top). Intervals between samples do not represent true stratigraphic thicknesses, and the samples are not representative of core lithology between sampling points.

Core depth	Description
110–114.3 m	Non-aligned <4 cm intraclasts of white chert with gray, sparsely spherule-bearing, micro-fragmental matrix
109.9–110 m	Poorly aligned <4 cm intraclasts of white to gray chert interspersed with gray, sparsely spherule-bearing, micro-fragmental matrix
88.1–88.3 m	Poorly aligned <3 cm intraclasts of white to gray chert interspersed with gray micro-fragmental matrix; infrequent spherules
84.45–84.6 m	Aligned <7 cm intraclasts of white to gray chert within gray spherule-bearing micro-fragmental matrix
84.1–84.25 m	Aligned <2 cm intraclasts of white to gray chert interspersed with gray spherule-bearing micro-fragmental matrix
83.4–83.6 m	Blocks of gray chert interspersed with pockets of spherule-bearing micro-fragmental matrix
77.1–77.8 m	Spherule layer: flattened aligned white chert intraclasts within a matrix containing densely packed mm-scale spherules
74.4–74.5 m	Flattened aligned gray chert intraclasts (>10 cm) interspersed with micro-fragmental spherule-bearing matrix
69–69.1 m	Angular chert fragmentals with up to <10 cm large fragments interspersed with mm-scale spherule-bearing granular matrix
65.2–65.35 m	Banded gray and black chert interspersed with mm-scale spherule-bearing granular matrix
57–58.1 m	Spherule layer: angular chert fragmentals with up to <7 cm large fragments adjacent to granular matrix containing densely packed mm-scale spherules

Table 2
Whole rock analytical data (XRF and ICPMS) for major oxides and key trace elements from MBCM spherule-rich samples at 57.1 m and 58.1 m.

Sample at 57.1 m; Geoscience Australia				Sample at 58.1 m; Genalysis Laboratories			
Method – XRF	%	Method – ICPMS	ppm	ICPMS	%	ICPMS	ppm
SiO_2	99.16	Ni	17.3			Ni	54
TiO_2	0.02	Cr	7.5	TiO_2	0.003	Cr	<5
Al_2O_3	0.52	V	10.4	Al_2O_3	0.07	Co	12.1
Fe_2O_3	0.1	Cu	1.77	Fe_2O_3	6.30	V	2
MnO				MnO	0.20	Cu	3
MgO				MgO	0.81	NIS collection ICPMS	ppb
CaO	0.01			CaO	0.048	Au	5
Na_2O	0.04			Na_2O	0.006	Pd	4
K_2O	0.08			K_2O	<0.003	Pt	6
P_2O_5				P_2O_5	<0.011	Re	5
Total	99.9					Rh	1
						Ru	6
						Os	3
						Ir	2
Ni/Cr			2.3				10.8
Pd/Ir							2.0

what appear to be the inner zones of spherules (Fig. 12). Plots of Ni–Cr show a distinction between the distributions of the siderophile trace elements in the spherules, in particular in the rims, compared to Ni–Cr relationships in mafic and ultramafic volcanic rocks (Fig. 11; Appendix G). Ni levels in Fe-rich rims can be >200 ppm and Ni/Cr ratios are commonly >10, and in some samples up to 51 (Fig. 12; Appendix E). A clear polarity is apparent in spherule rims between low Ni zones (Ni < 90 ppm) and high-Ni zones (Ni ~ 150–250 ppm; (Fig. 12). Ni levels in internal quartz-dominated spherule zones are mostly below detection levels for Ni > 0.5 ppm and Cr ->0.6 ppm.

The high Ni levels and exceptionally high Ni/Cr ratios in spherule rims (Figs. 11 and 12) may represent a chondritic component (chondrites Ni/Cr = 3.96; mantle Ni/Cr = 0.74; oceanic crust Ni/Cr = 0.52; continental crust Ni/Cr = 0.69), potentially offering a discrimination between terrestrial materials and material contaminated with a chondrite component (Appendix G). Comparisons of Ni/Cr ratios between (a) whole rock compositions and Fe-rich spherule rim compositions and (b) peridotitic komatiites, high-Mg basalts and tholeiitic basalts from the Barberton greenstone belt and Warrawoona greenstone belts and komatiite analyses from several terrains (Fiorentini et al., 2011; Appendix G), indicates clear distinction between the field of MBCM spherules (Ni/Cr ratios mostly in the range of ~4.4–17.4) (Appendix G3) and mafic igneous compositions of (Ni/Cr ratios mostly ~0.17–1.09) (Fig. 11a and b; Appendix G5 and G6).

7. PGE anomalies

The abundance of Ir in chondrites (455 ppb, Appendix G), which exceeds mantle levels (3.2 ppb) by more than two orders of magnitude ($Ir_{chondrite}/Ir_{mantle}$ = 142) (Appendix G), allows detection of meteoritic components even where strongly diluted by a terrestrial crustal component. The higher ratio of the relatively mobile Pd to the relatively refractory Ir in terrestrial rocks (komatiites: Pd/Ir mostly > 3.0; chondrites Pd/Ir ~ 1.2) furnishes a criterion for identification of a chondritic component in the ejecta.

Kyte et al. (1992), Byerly and Lowe (1994), Lowe et al. (2003), studied the PGE (Pd, Pt Os, Ir), Au, and isotopic compositions in Ni-rich spinels and PGE-nano-nuggets of Barberton spherules, noting exceptionally high PGE levels and PGE chondrite-normalized ratios compared to sediments of known or suspected impact origin. The lack of primary phases and the high-degree of silicification in the MBCM spherules restrict investigations of the PGEs to the

Table 3
LA-ICPMS analyses of siderite in spherule rims. Sample at 57.1 m. The locations of the pit burn point analyses are indicated in Fig. 10b. Analyses performed at RSES. EMP values used in calibration are given in Appendix B.

	Sc	2se	Ti	2se	V	2se	Cr*	2se	Co	2se	Ni*	2se	Cu	2se	Zn	2se	Ni/Cr	Ni/Co
Values in ppm																		
#1	85	4	32	12	53	10	15	4	17	1	150	25	42	6	356	61	10.0	9
#2	39	9	12	7	8	1	5	3	9	1	55	21	24	8	346	39	11.0	6
#3	56	6	35	10	9	4	5	3	9	1	87	33	37	12	529	87	17.4	10
#4	70	8	27	19	53	9	18	3	11	2	87	24	44	6	386	20	4.8	8
#5	112	16	144	92	71	17	23	8	10	2	102	33	38	7	271	39	4.4	10
#6	62	7	35	16	49	12	15	6	22	1	165	36	18	5	265	28	11.0	8
#7	29	5	33	12	22	3	5	2	14	1	90	13	25	2	298	15	18.0	6
#8	12	1	12	7	10	0	17	26	10	0.5	64	8	15	1	259	8	3.8	6
#9	42	5	12	3	9	1	6	2	15	1	64	15	103	9	470	34	10.7	4
#10	11	0.5	1	1	6	0.4	2	1	6	0.3	33	7	5	0.3	147	6	16.5	6

* Detection limits: Ni – 0.5; Cr – 0.6.

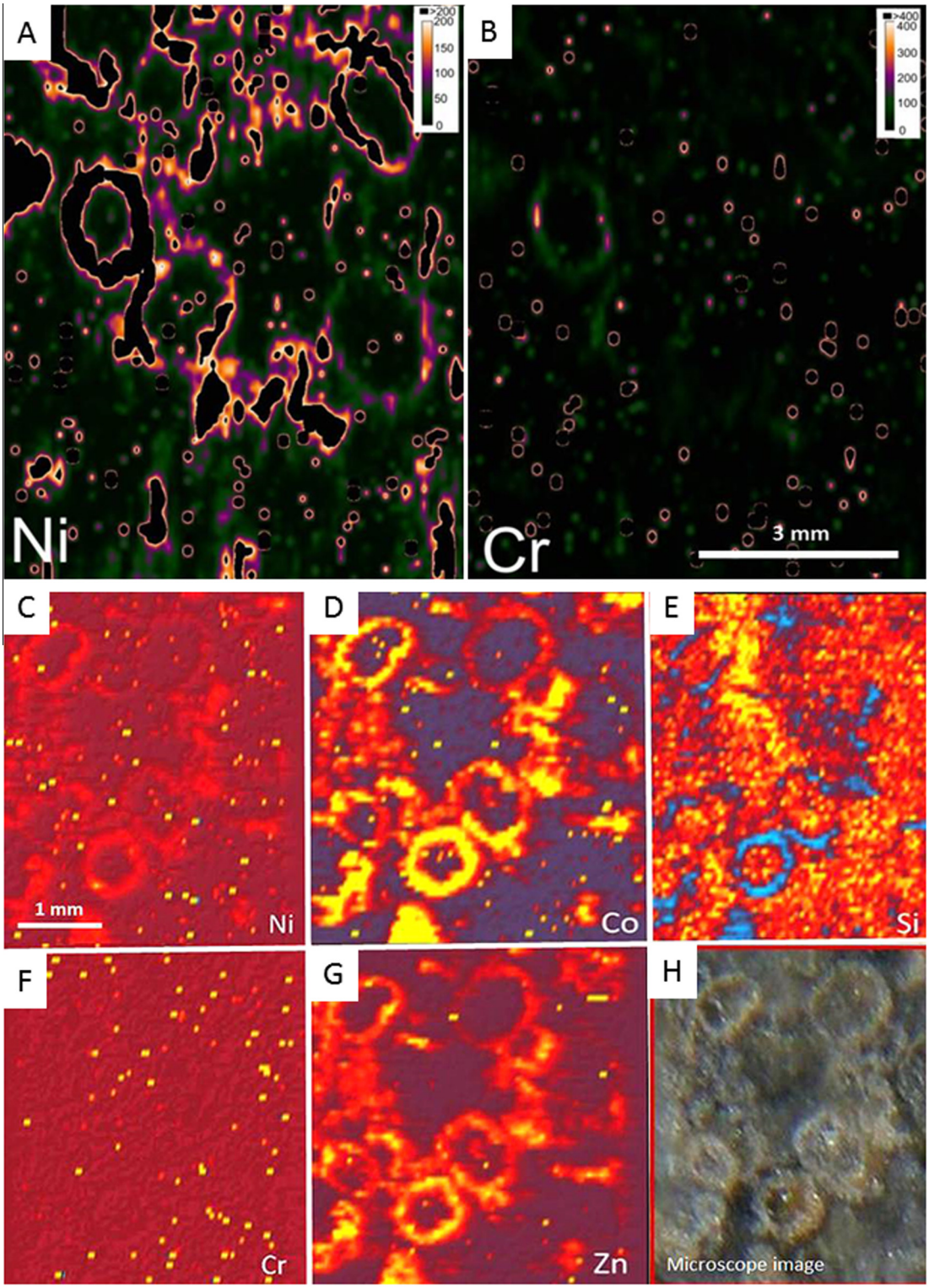

Fig. 9. (A and B) Laser ICPMS counts image of Ni and Cr in sample 58.1 m. (C–G) Laser ICPMS counts per-second maps for Ni, Co, Si, Cr and Zn. Sample 58.1 m, background subtracted. High counts for each element in yellow, low counts in blue. (H) Microscopic image of the analytical site scanned in images C–G. (For interpretation of the references to colour in this figure legend, the reader is referred to the web version of this article.)

whole rock analysis (Table 2) and LA-ICPMS analysis of siderite at the spherule rims (Appendices C, E, F and G3). As indicated by the analyses, whereas the concentrations of the PGEs vary in connection with secondary alteration processes, chondrite-normalized ratios of the relatively volatile PGE (Pd) to relatively refractory PGE (Ir) and high Os/chondrite ratios are permissible of a meteoritic component.

PGE whole rock analysis by the NiS collection fire essay method (Table 2) reveals exceptionally high PGE contents for a rock composed of ~93% SiO_2 (approximate SiO_2 based on contents of the other oxides). Pd at 4 ppb (detection limit of 1 ppb) and Ir at 2 ppb (detection limit of 1 ppb) give a Pd/Ir ratio of 2.0. This ratio is very different from that of oceanic basalts (Fig. 13a) and is somewhat lower than the Pd/Ir ratios of ~2.7–11.2 of high-Mg

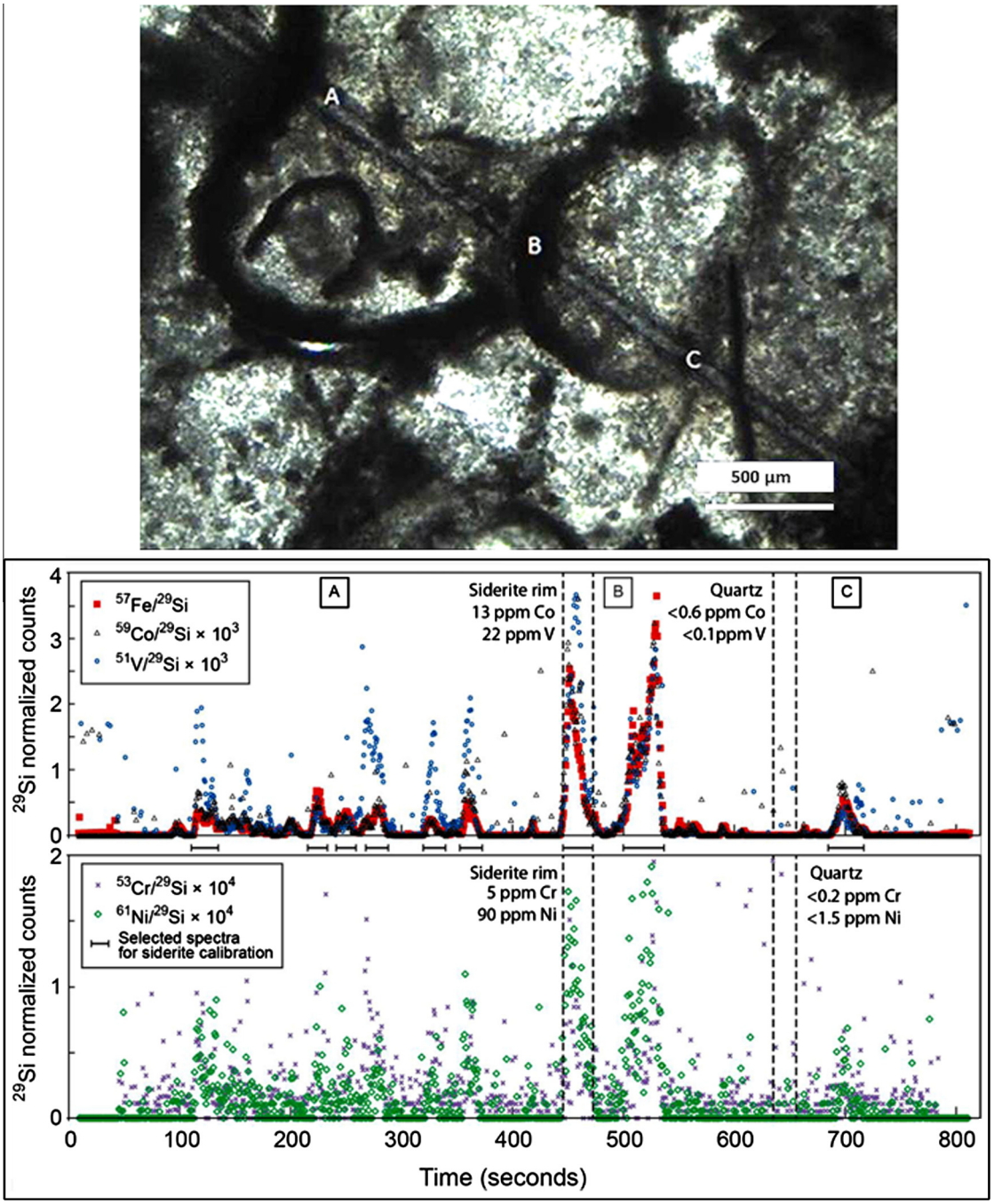

Fig. 10. (a) Laser ICPMS image of spherules from drill hole ABDP 1 depth 57.1 m transected by laser ICPMS; (b) time-resolved spectra of LA-ICP-MS analysis of a transect through spherules from drill hole ABDP 1 samples 57.1 m. Representative sections of the spectra for calibrating the compositions of siderite and quartz are shown in dotted lines. Short lines underlying the Fe–Co–V trends indicate calibrated pit burn points presented in Table 3.

peridotitic komatiite (Pd ~ 1.9–12.8 ppb; Ir ~ 0.26–2.13 ppb; Fiorentini et al., 2011).

The absolute levels of the PGEs and of trace metals in the spherule rims are unlikely to represent original abundance levels in the source rocks of the spherules. In the case of impact spherules this variation is due to fractionation associated with vaporization and condensation. LA-ICPMS pit analyses of spherules of sample 58.1 m allow comparisons of the relations between the relatively more refractory PGE (Os, Ru, Rh), the more volatile PGE (Pd, Pt) and Au and chondritic C1 compositions. The examination of the PGE relations indicates high refractory to volatile chondrite-normalized PGE ratios (Fig. 13). Although the primary Pd/Ir ratios of the spherules are unknown, the relatively high Os/chondrite and Rh/chondrite ratios and lower Pt/chondrite, Pd/chondrite and Au/chondrite ratios hint at relative enrichment of some of the more refractory PGEs and/or relative depletion of the more volatile PGEs (Fig. 13b); Appendix G).

Comparisons can be made between the PGE contents of the MBCM sample at 58.1 m and PGE values reported from the Spherule Marker Bed, Wittenoom Formation (Simonson et al., 2009) (Ir 0.49–0.68 ppb; Pd/Ir 5.2–7.2), the Carawine Dolomite megabreccia (Simonson et al., 1998) (Ir 0.60–1.54 ppb; Pd/Ir 2.4–6.2), the Monteville Formation (Simonson et al., 2000, 2009) (Ir ~ 4.9 ppb; Pd ~ 6.8 ppb; Pd/Ir ~ 1.4), Dales Gorge (Ir ~ 1.13–17.9;

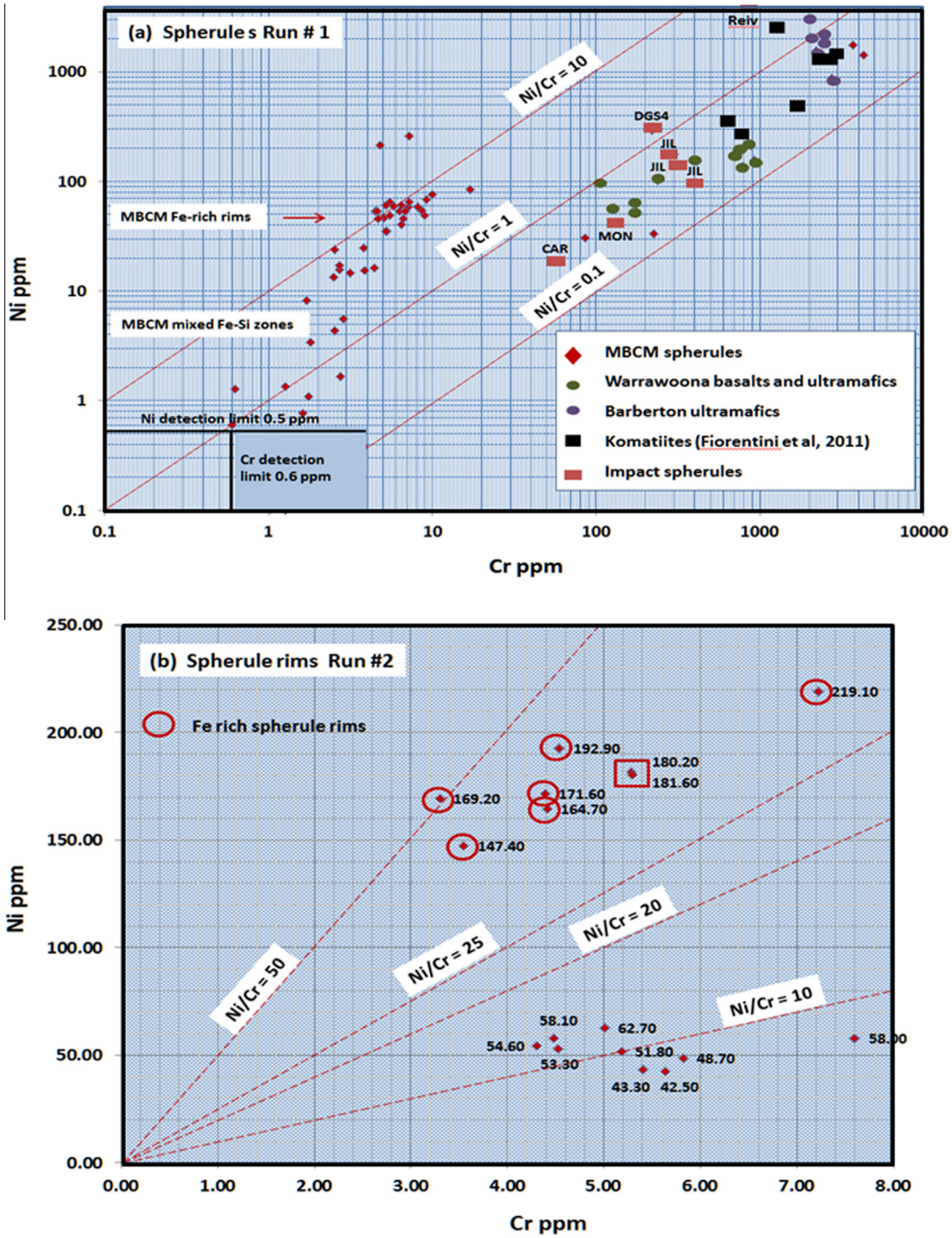

Fig. 11. (a) Ni–Cr relations in rims and cores of spherules in sample 58.1 m compared with komatiites, basalts and impact spherule-bearing samples. Note the bimodal distribution of MBCM Ni–Cr values between high Ni and high Ni/Cr rims and low Ni and Ni/Cr spherule interiors. (b) Ni–Cr relations in Fe-rich spherule rims in sample 58.1 m compared with komatiites, basalts and impact spherule-bearing samples. Note the bimodal distribution of Ni levels in the spherules, i.e. the Ni content of the siderite rim of the spherule in plot (a) is 3–5 times higher than the Ni in rims of other spherules in the MBCM, whereas the Cr content of different rims is relatively constant. Note that whereas the Ni content of the siderite rim of the spherules spans a wide range of ~50–220 ppm, the Cr content of different rims is relatively more constant at ~3–20 ppm.

Pd/Ir ~ 0.56–1.40) and JIL (Ir ~ 5.18–11.8; Pd/Ir ~ 0.77–1.53) (Appendix G). The confirmed impact spherule units display a wide variation of the PGE levels, including near-chondritic values for well-preserved spherules of the Monteville Formation and high Pd/Ir rations for the SMB and Carawine spherules. The Pd/Ir ratios in the latter units (Appendix G) suggests alteration-related enrichment of Pd relative to Ir. With this perspective the relatively low Pd/Ir ratio of 2.0 of the MBCM spherules provides support for a relict meteoritic component.

8. Discussion

Examination of the ABDP 1 core, drilled through the Marble Bar Chert Member, has identified spherule-bearing chert and chert

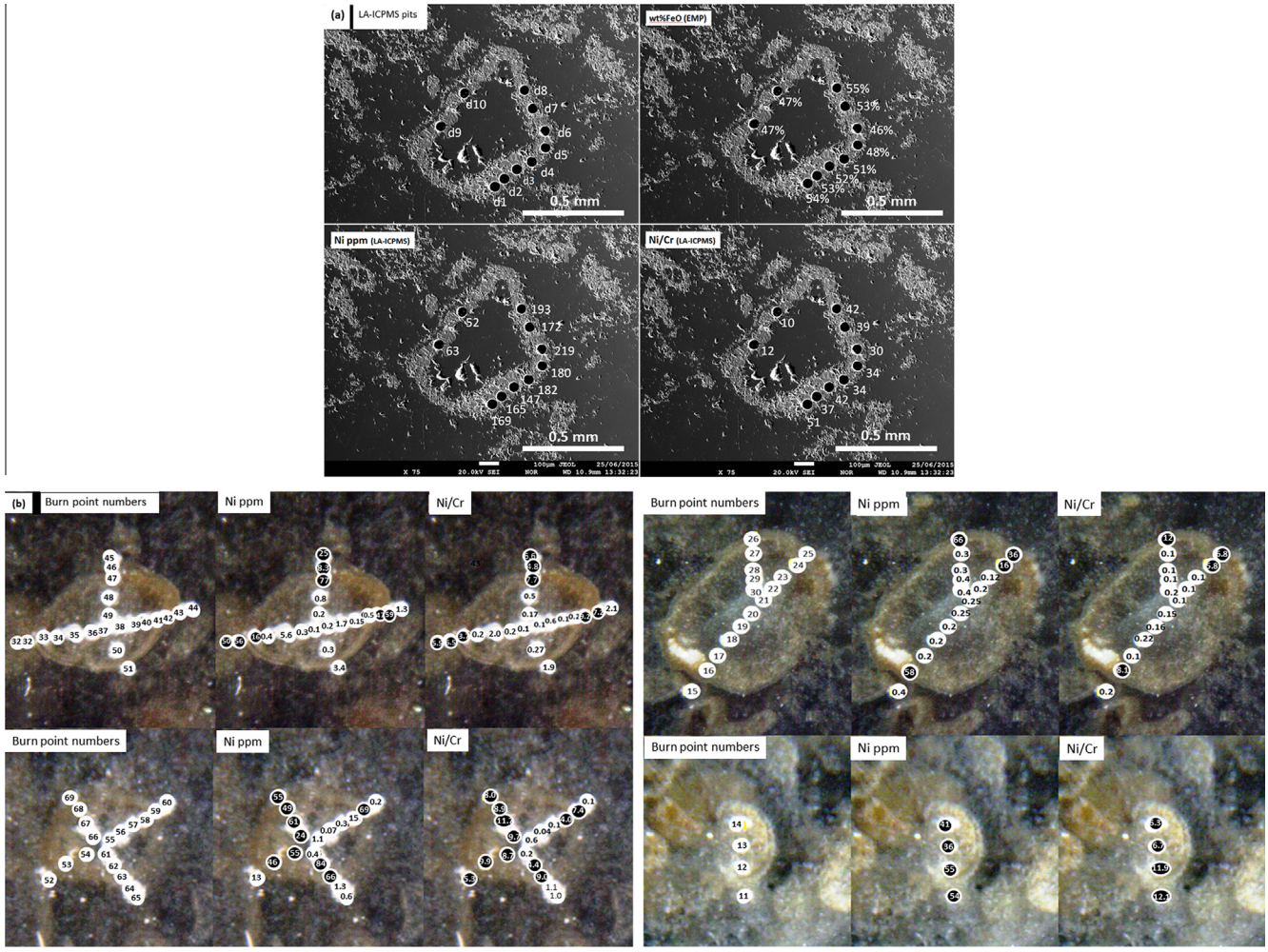

Fig. 12. (a) LA-ICPMS analytical points through the rims of spherules in sample 58.1 m calibrated by EMP measurements, displaying the EMP analytical point numbers. FeO levels, Ni levels and Ni/Cr ratios. (b). EMP-calibrated LA-ICPMS burn points (pits) along cross sections through spherules of sample 58.1 m. High Ni and Ni/Cr values in the lower row of images indicate a section cut close to a spherule margin.

breccia, part of which is interpreted as diamictite, in Zones 1 and possibly in parts of Zone 2 (Fig. 3). High concentrations of spherule-bearing arenite matrix are observed at 57–58 m and at 77 m whereas at other levels spherules are more dispersed. At most levels and in particular in Zone 2 the diamictite contains dark gray hydrothermal chert in layers and veins engulfing and injected into angular blocks of bedded chert.

Despite extensive silicification which overprints primary textures, and variable hydrothermal activity, the MBCM diamictite displays distinct sedimentological and textural analogies with platy chert breccia-hosted impact spherules documented in the Antarctic Creek Member (Lowe and Byerly, 1986; Lowe et al., 1989; Glikson et al., 2004) and the Jeerinah Impact Layer (Simonson et al., 2001).

Sedimentary concretions, which reach larger size distributions than the MBCM spherules, suggest derivation from an external source. The MBCM spherules are unlikely to be correlated with sedimentary silica granules, which are mostly oblate at dimensional ratios up to 4:1 and texturally distinct from microkrystite spherules (Stefurak et al., 2014). Silica granules are not known to have the high trace metals and high Ni/Cr ratios typical of microkrystite spherules (Fig. 11). The textural features of the spherule-bearing units do not accord with those of volcanic lapilli, varioles and ocelli (Ferguson and Currie, 1972). Volcanic ocelli, common in komatiitic basalts and in pillow lavas, vary in size up to several centimeters. Volcanic varioles display outward radiating quench crystallites commonly centered on feldspar or quartz crystals (Fig. 4). Volcanic accretionary lapilli are commonly larger than a millimeter and display well defined concentric zonation.

The dense packing of spherules at core levels 57–58 m and 77 m, separated by about 20 m of chert (14 m true stratigraphic thickness), is suggestive of two separate spherule-forming events. An alternative interpretation, that the concentration of spherules at 77 m was the result of current-driven dispersal of the spherules at the 57–58 m level, would require extremely rapid deposition (equivalent to the duration of tsunami activity) of the intervening 14 m succession. In the first interpretation, estimates of the rate of sedimentation of the 14 m of chert separating the dense spherule concentrations may help to constrain the age difference between the two events. Independent estimates for the depositional rates in the Hamersley Group based on U–Pb zircon dating, reviewed by Trendall et al. (2004), suggest rates in the range of 33–180 m per 1 million years for banded iron formations and much slower depositional rates for shales and carbonates (between 5 and 12 m per million years). If the maximum rate for deposition of BIF (~180 m per 1 million years) is applied to the ~14 m of chert + arenite interval separating the high concentrations of spherules in the MBCM, the two depositional events would be separated by a time interval of ~0.1 million years. If the banded chert is interpreted as silicified shale, the time interval might have been up to 3 million years.

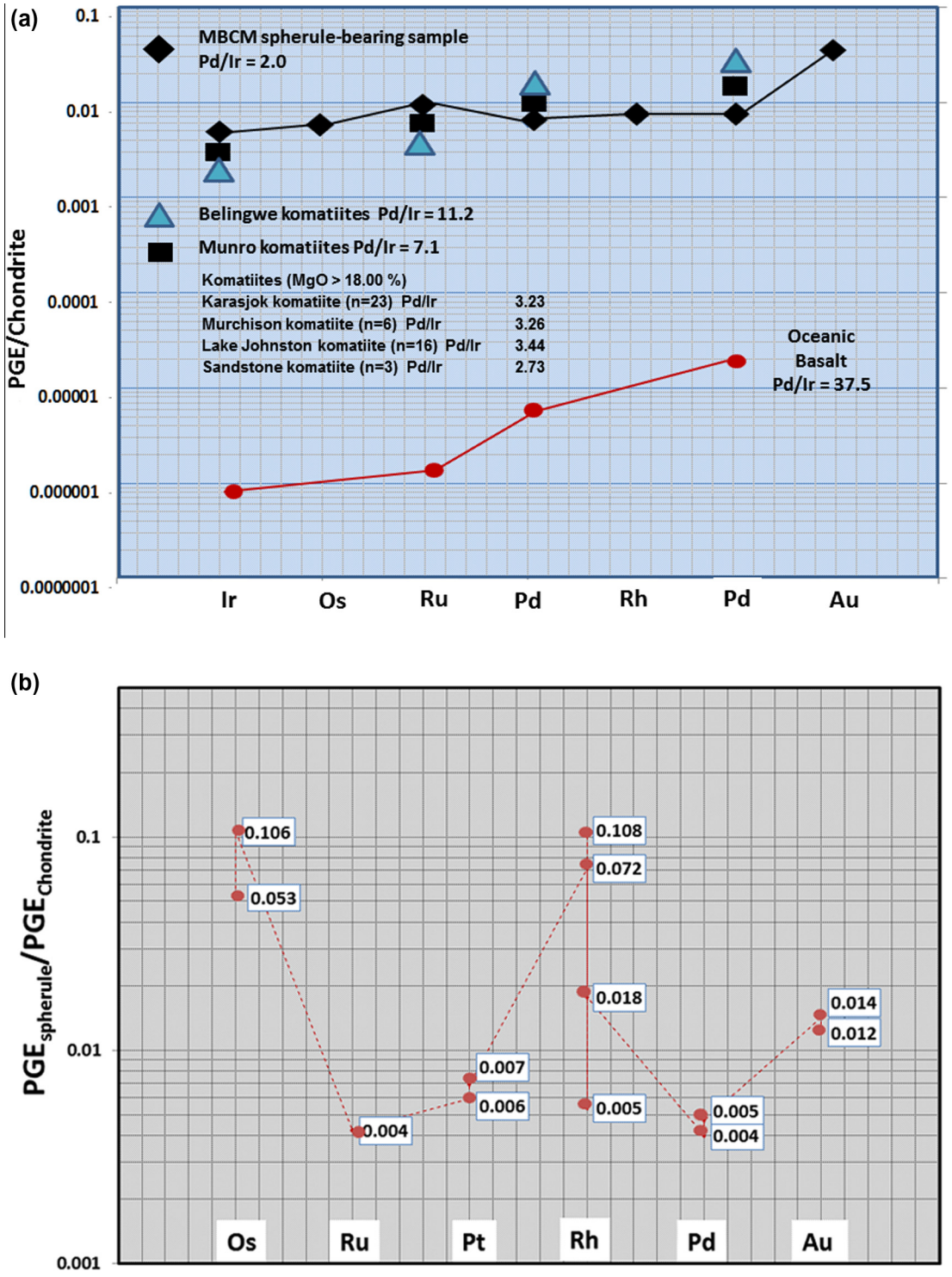

Fig. 13. (a) Chondrite-normalized PGE plots in MBCM sample 58.1 m compared to oceanic basalt, Belingwe and Munro komatiites (Rehkamper et al., 1999) and average peridotite komatiite (MgO > 18%) (Fiorentini et al., 2011). Data from Table 3 and Appendix G. Data source for chondrite: (McDonough and Sun, 1995); (b) Chondrite-normalized plot of Os, Ru, Pt, Rh, Pd and Au analyzed by laser-ICPMS in the rims of sample 58.1 m. Anomalously high values of Pd (Appendix F) are not included.

Whereas the absolute levels of PGE and trace metals and the PGE can be highly variable (Appendix G), their ratios outline more consistent patterns. The high Ni/Cr and low volatile/refractory PGE ratios (Fig. 11) suggest a relative coherence of some of the siderophile and PGE elements. Comparisons of Ni/Cr ratios of impact ejecta units and mafic and ultramafic volcanic rocks (Fig. 13) can potentially be used for estimates of the chondritic component in ejecta. Likewise, $Ni_{spherules}/Ni_{chondrite}$ and $Ir_{spherule}/Ir_{chondrite}$ ratios can be used for estimates of the composition of the source target materials. Ni and Ir spherule/chondrite ratios of impact ejecta units range from high (Reivilo spherules $Ir_{spherule}//Ir_{chondrite} \sim 0.57$; $Ni_{spherules}/Ni_{chondrite} \sim 0.37$), to moderate (Dales Gorge DGS4 spherules $Ir_{spherule}/Ir_{chondrite} \sim 0.039$; $Ni_{spherules}/Ni_{chondrite} \sim 0.028$) (Appendix G), to very low in the MBCM spherules ($Ir_{spherule}/Ir_{chondrite} \sim 0.0043$; $Ni_{spherules}/Ni_{chondrite} \sim 0.005$), as calculated from whole rock Ni and Ir compositions. However, the highly altered

state of the MBCM siderite-quartz spherules places limits on the reliability of such estimates.

The abnormally high Ni/Cr of some spherule rims, as compared to average chondrites, may suggest the Ni and Cr contributions came from a CH-chondrite (Ni/Cr 8.3, Glass and Simonson, 2013) or from an M-Type iron rich asteroid, such as for example 21-Lutetia or 22-Kalliope (Vernazza et al., 2011). Metallic microkrystite spherules are relatively rare in impact ejecta, although high-Fe occur in the JIL ejecta with spherule units >20% Fe_2O_3 (Simonson et al., 2009) and in stilpnomelane-rich DGS4 spherules (Glikson and Allen, 2004). In the latter case secondary enrichment in iron leached from the associated banded iron formations is likely.

Most studies of the MBCM have emphasized the extensive hydrothermal alteration of its protoliths (sandstone, siltstone, shale, diamictite, fine-grained volcaniclastic sediments, basaltic tuff, basalt, and carbonate sediments). Primary silica precipitates adjacent to hydrothermal vents (Hoashi et al., 2009) may also be present. Orberger et al. (2006) and Van Kranendonk (2006) suggested that the hydrothermal fluids were derived from basalt sources. Basaltic units spatially associated with the MBCM are unlikely to form the source of the PGEs in view of the high PGE levels and the distinctly low ratios of volatile to refractory PGEs in the latter.

The intimate association of spherule-rich arenite with platy chert fragments (Fig. 4) militates for concomitant condensation and settling of silicate melt droplets, and sea floor excavation by seismic disturbance and tsunami waves. Moreover, as noted previously, the diamictite in Zone 1 is entirely composed of clasts from within the MBCM. This contrasts with diamictite at a different stratigraphic level at Marble Bar Pool where Olivier et al. (2012) reported basaltic and granitic clasts within turbidity current deposits in the channel of a submarine fan. Examples of similar relations in spherule-bearing diamictite spherules in the Pilbara include: (1) the Antarctic Creek Member (ACM) spherule units, North Pole area of the east Pilbara (3470.1 ± 1.9 Ma- Byerly et al., 2002), displaying spherule-rich matrix interspersed with chert intraclasts; (2) Jeerinah Impact layer, Fortescue Group (2629 ± 5 Ma Nelson, 1999) (Simonson et al., 2001; Glikson and Hickman, 2014), displaying a spherule-rich units containing brown argillite intraclasts above the Roy Hill Member, and (3) blocks of carbonate and chert in the Carawine Dolomite megabreccia (Glikson, 2004).

Stratigraphic and isotopic age data (Hickman and Van Kranendonk, 2004; Hickman and Van Kranendonk, 2004, 2008; Hickman, 2012) allows distinction between the ~3.46–3.45 Ga MBCM ejecta unit and a ~3.47 Ga ejecta units in the Antarctic Creek Member located approximately 40 km to the west of Marble Bar.

The size of the asteroid which triggered the MBCM impact event may be modeled from spherule diameters. A linear relation exists between spherule sizes and impactor size and a complex relation between spherule size and impact velocity (Melosh and Vickery, 1991; Kyte et al., 1992, 2003; Johnson and Melosh, 2012). For example, impact by a 10 km-large asteroid at a velocity of ~21 km/s would result in condensation of spherules approximately ~250 μm in diameter, i.e. similar to those formed by the K–T boundary impact (Johnson and Melosh, 2012). According to Melosh and Vickery (1991) spherules on the order of ~2000 μm correspond to impact by projectile as large as 40 km in diameter. It would follow from the above that the upper 2 mm-diameter of the MBCM spherules (Fig. 6) implies a very large asteroid impact, which warrants further search for possible volcanic and/or tectonic effects of the event.

9. Conclusions

A new impact ejecta unit has been discovered in the ~3.46–3.45 Ga Marble Bar Chert Member, Duffer Formation, Warrawoona Group, Pilbara Craton, Western Australia, consisting of almost totally silicified spherules with Fe-rich rims within an arenite matrix of a chert-plate diamictite. Evidence for an impact origin arises from:

A. The highly spherical forms of the spherules.
B. A spherules size distribution in a range of mostly 1–2 mm.
C. Iron-rich and trace metal rich composition of spherule rims.
D. The high Ni and Ni/Cr composition of the spherules and in particular siderite grains at the spherule rims.
E. High whole rock Ir level and low Pd/Ir ratio.
F. The presence of the spherules in the matrix of a sedimentary chert-plate diamictite, by analogy to diamictite-hosted impact ejecta, representing impact-related tsunami deposits.

Dense concentrations of spherules at the 57–58 m level and the 77 m level of the core, separated by banded chert, raise the possibility of two distinct impact events. The occurrence of impact ejecta units 3472 Ma-old in the Barberton greenstone belt and 3470 Ma and 3459–3449 Ma in the east Pilbara Craton defines large mid-Archean asteroid impacts, with implications for early crustal evolution.

Acknowledgements

We thank David DiBugnara (Geoscience Australia) for SEM–EDS analyses of spherules, John Vickers for preparation of thin sections and Brad McDonald for assistance with LA-ICPMS. The authors acknowledge the facilities, and the scientific and technical assistance, especially Malcolm Roberts, of the Australian Microscopy & Microanalysis Research Facility at the Centre for Microscopy, Characterization & Analysis, The University of Western Australia, a facility funded by the University, State and Commonwealth Governments. Samples of the ABDP 1 core used in the study were provided by the Perth Core Library of the Geological Survey of Western Australia (GSWA). Arthur Hickman and Sandra Romano publish with permission of the Executive Director of the GSWA. We thank Balz Kamber and three reviewers for their constructive comments and suggestions.

Appendix A–G. Supplementary data

Supplementary data associated with this article can be found, in the online version, at http://dx.doi.org/10.1016/j.precamres.2016.04.003.

References

Byerly, G.R., Lowe, D.R., 1994. Spine1 from Archean impact spherules. Geochim. Cosmochim. Acta 58, 3469–3486.
Byerly, G.R., Lowe, D.R., Wooden, J.L., Xie, X., 2002. An Archean impact layer from the Pilbara and Kaapvaal cratons. Science 297, 1325–1327.
Buick, R., Thornett, J.R., McNaughton, N.J., Smith, J.B., Barley, M.E., Savage, M., 1995. Record of emergent continental crust ~3.5 billion years ago in the Pilbara Craton of Australia. Nature 375, 574–577.
De Vries, S.T., Nijman, W., Wijbrans, J.R., Nelson, D.R., 2006. Stratigraphic continuity and early deformation of the central part of the Coppin Gap Greenstone Belt, Pilbara, Western Australia. Precambr. Res. 147, 1–27.
DiMarco, M.J., Lowe, D.R., 1989. Stratigraphy and sedimentology of an Early Archean felsic volcaniclastic sequence eastern Pilbara Block Western Australia with special reference to the Duffer Formation and implications for crustal evolution. Precambr. Res. 44, 147–169.
Eggins, S.M., Woodhead, J.D., Kinsley, L.P.J., Mortimer, G.E., Sylvester, P., McCulloch, M.T., Hergt, J.M., Handler, M.R., 1997. A simple method for the precise determination of >40 trace elements in geological samples by ICPMS using enriched isotope internal standardization. Chem. Geol. 134, 311–326.
Ferguson, J., Currie, K., 1972. Silicate Immiscibility in the Ancient "Basalts" of the Barberton Mountain Land, Transvaal. Nat. Phys. Sci. 235, 86–89.
Fiorentini, M.L., Barnes, S., Maier, W.D., Burnham, O.M., Heggie, G., 2011. Global variability in the platinum-group element contents of komatiites. J. Petrol. 52, 83–112.

Glass, B.P., Burns, C.A., 1988. Microkrystites: a new term for impact-produced glassy spherules containing primary crystallites. Proc. Lunar Planet. Sci. Conf. 18, 455–458.
Glass, B.P., Simonson, B.M., 2013. Spherule layers near the archean-proterozoic boundary. Distal impact ejecta layers. Impact Stud. 2013, 419–497.
Glikson, A.Y., 2004. Early Precambrian asteroid impact-triggered tsunami: excavated seabed debris flows exotic boulders and turbulence features associated with 3.47–2.47 Ga-old asteroid impact fallout units, Pilbara Craton, Western Australia. Astrobiology 4, 1–32.
Glikson, A.Y., 2014. The Archean: Geological and Geochemical Windows into the Early Earth. Springer, Dordrecht, p. 238.
Glikson, A.Y., Allen, C., 2004. Iridium anomalies and fractionated siderophile element patterns in impact ejecta, Brockman Iron Formation, Hamersley Basin, Western Australia: evidence for a major asteroid impact in simatic crustal regions of the early Proterozoic earth. Earth Planet. Sci. Lett. 20, 247–264.
Glikson, A.Y., Hickman, A.H., 2014. Coupled asteroid impacts and banded iron-formations, Fortescue and Hamersley Groups, Pilbara, Western Australia. Aust. J. Earth Sci. 61, 689–701.
Glikson, A.Y., Vickers, J., 2005. The 3.26–3.24 Ga Barberton asteroid impact cluster: tests of tectonic and magmatic consequences, Pilbara Craton, Western Australia. Earth Planet. Sci. Lett. 241, 11–20.
Glikson, A.Y., Vickers, J., 2010. Asteroid impact connections of crustal evolution. Aust. J. Earth Sci. 57, 79–95.
Glikson, A.Y., Allen, C., Vickers, J., 2004. Multiple 3.47 Ga-old asteroid impact fallout units, Pilbara Craton, Western Australia. Earth Planet. Sci. Lett. 221, 383–396.
Green, M.G., Sylvester, P.J., Buick, R., 2000. Growth and recycling of early Archaean continental crust: geochemical evidence from the Coonterunah and Warrawoona Groups, Pilbara Craton, Australia. Tectonophysics 322, 69–88.
Hickman, A.H., 2005. Evidence of early life from international collaborative drilling in the Pilbara Craton. Western Aust. Geol. Surv. Ann. Rev. 2004–05, 27–32.
Hickman, A.H., 2008. Regional review of the 3426–3350 Ma Strelley Pool Formation, Pilbara Craton, Western Australia, Record 2008/15. Geological Survey of Western Australia, 27p.
Hickman, A.H., 2012. Review of the Pilbara Craton and Fortescue Basin, Western Australia: Crustal evolution providing environments for early life. Island Arc 21, 1–31.
Hickman, A.H., VanKranendonk, M.J., 2004. Diapiric processes in the formation of Archean continental crust, East Pilbara Granite-Greenstone Terrane, Australia. In: Eriksson, P.G., Altermann, W., Nelson, D.R., Mueller, W.U., Catuneanu, O. (Eds.), The Precambrian Earth: Tempos and Events in Precambrian Time, Developments in Precambrian Geology 12. Elsevier, Amsterdam, pp. 118–139.
Hickman, A.H., Van Kranendonk, M.J., 2008. Archean crustal evolution and mineralization of the northern Pilbara Craton – a field guide. Geol. Surv. Western Aust. Rec. 13, 1–79.
Hickman, A.H., Van Kranendonk, M.J., 2012. Early Earth evolution: evidence from the 3.5–1.8 Ga geological history of the Pilbara region of Western Australia. Episodes 35, 283–297.
Hoashi, M., Bevacqua, D.C., Otake, T., Watanabe, Y., Hickman, A.H., Utsunomiya, S., Ohmoto, H., 2009. Primary hematite formation in an oxygenated sea 3.46 billion years ago: Nature. Geosciences 2, 301–306.
Isozaki, Y, Maruyama, S, Kimura, G, 1991. Middle Archean (3.3 Ga) Cleaverville accretionary complex in Northwestern Pilbara Block, Western Australia. In: Eos 72, 542.
Jochum, K.P. et al., 2011. Determination of reference values for NIST SRM 610–617 glasses following ISO guidelines. Geostand. Geoanal. Res. 35 (4), 397–429.
Johnson, B.C., Melosh, H.J., 2012. Formation of spherules in impact produced vapour plumes. Icarus 217, 416–430.
Jones, A.P., Price, D.G., De Carli, P.S., Price, N., Clegg, R., 2003. Impact decompression melting: a possible trigger for impact induced volcanism and mantle hotspots? In: Koeberl, P.C., Martinez-Ruiz, F.C. (Eds.), Impact Markers in the Stratigraphic Record, Impact Studies. Springer-Verlag, Berlin Heidelberg, pp. 91–119.
Kato, Y., Nakamura, K., 2003. Origin and global tectonic significance of Early Archean cherts from the Marble Bar greenstone belt, Pilbara Craton, Western Australia. Precambr. Res. 125, 191–243.
Kato, Y., Suzuki, K., Nakamura, K., Hickman, A.H., Nedachi, M., Kusakabe, M., Bevacqua, D.C., Ohmoto, H., 2009. Hematite formation by oxygenated ground water more than 2.76 billion years ago. Earth Planet. Sci. Lett. 278, 40–49.
Kemp, A.I.S., Hickman, A.H., Kirkland, C.L., 2015. Early evolution of the Pilbara Craton from hafnium isotopes and inherited zircons: Geological Survey of Western Australia, Report 151, 26p.
Kimura, G., Maruyama, S., Isozaki, I., 1991. Early Archean accretionary complex in the eastern Pilbara Craton, Western Australia – detailed field occurrence in the Marble Bar area. Eos 72, 542.
Kitajima, K., Maruyama, S., Utsunomiya, S., Lio, J.G., 2001. Seafloor hydrothermal alteration at an Archean mid-ocean ridge. J. Metamorph. Geol. 19, 583–599.
Kjellgren, G.M., 1976. The Marble Bar chert, and its geological setting, Marble Bar, Pilbara Block, W.A.: University of Western Australia B.Sc. (Hon.) thesis (unpublished).
Kojima, S., Hanamuro, T., Hayashi, K., Haruna, M., Ohmoto, H., 1998. Sulphide minerals in Early Archean chemical sedimentary rocks of the eastern Pilbara district, Western Australia. Mineral. Petrol. 64, 219–235.
Komiya, T., Maruyama, S., Hirata, T., Yurimoto, H., 2002. Petrology and geochemistry of MORB and OIB in the mid-Archean North Pole Region, Pilbara Craton, Western Australia: implications for the composition and temperature of the upper mantle at 3.5 Ga. Int. Geol. Rev. 44, 988–1016.
Kyte, F.T., Zhou, L., Lowe, D.R., 1992. Noble metal abundances in an early Archean impact deposit. Geochim. Cosmochim. Acta 56, 1365–1372.
Kyte, F.T., Shukolyukov, A., Lugmair, G.W., Lowe, D.R., Byerly, G.R., 2003. Early Archean spherule beds: chromium isotopes confirm origin through multiple impacts of projectiles of carbonaceous chondrite type. Geology 31, 283–286.
Li, W., Czaja, A.D., Van Kranendonk, M.J., Beard, B.L., Roden, E.E., Johnson, C.M., 2013. An anoxic, Fe(II)-rich, U-poor ocean 3.46 billion years ago. Geochim. Cosmochim. Acta 120, 65–79.
Lowe, D.R., Byerly, G.R., 1986. Early Archean silicate spherules of probable impact origin, South Africa and Western Australia. Geology 14, 83–86.
Lowe, D.R., Byerly, G.R., 2010. Did LHB end not with a bang but a whimper. In: 41st Lunar and Planetary Science Conference (2010) 2563.pdf.
Lowe, D.R., Byerly, G.R., Asaro, F., Kyte, F.J., 1989. Geological and geochemical record of 3400 million year old terrestrial meteorite impacts. Science 245, 959–962.
Lowe, D.R., Byerly, G.R., Kyte, F.T., Shukolyukov, A., Asaro, F., Krull, A., 2003. Characteristics, origin, and implications of Archean impact-produced spherule beds, 3.47–3.22 Ga, in the Barberton Greenstone Belt, South Africa: keys to the role of large impacts on the evolution of the early Earth. Astrobiology 3, 7–48.
Lowe, D.R., Byerly, G.R., Kyte, F.T., 2014. Recently discovered 3.42−3.23 Ga impact layers, Barberton Belt, South Africa: 3.8 Ga detrital zircons, Archean impact history, and tectonic implications. Geology 42, 747–750.
McDonough, W.E., Sun, S., 1995. The composition of the Earth. Chem. Geol. 120, 223–253.
Melosh, H.J., Vickery, A.M., 1991. Melt droplet formation in energetic impact events. Nature 350, 494–497.
Minami, M., Shimizu, H., Masuda, A., Adachi, M., 1995. Two Archean Sm-Nd ages of 3.2 and 2.5 Ga for the Marble Bar Chert, Warrawoona Group, Pilbara Block, Western Australia. Geochem. J. 29, 347–362.
Nelson, D.R., 1999. Compilation of SHRIMP U–Pb zircon geochronology data, 1998. Western Aust. Geol. Surv. Rec. 2, 222.
Norrish, K., Chappell, B.W., 1977. X-ray fluorescence spectrometry. In: Zussman, J. (Ed.), Physical Methods in Determinative Mineralogy, second ed. Academic press, London, pp. 201–272.
Norrish, K., Hutton, J.T., 1969. An accurate X-ray spectrographic method for the analysis of a wide range of geological samples. Geochim. Cosmochim. Acta 33, 431–453.
Olivier, N., Dromart, G., Coltice, N., Flament, N., Rey, P., Sauvestre, R., 2012. A deep subaqueous fan depositional model for the PalaeoArchean (3.46 Ga) Marble Bar Cherts, Warrawoona Group, Western Australia. Geol. Mag. 149, 743–749.
Orberger, B., Rouchon, V., Westall, F., de Vries, S.J., Pinti, D.L., Wagner, C., Wirth, R., Hashizume, K., 2006. Microfacies and origin of some Archean cherts (Pilbara, Australia). In: Reimold, W.U., Gibson, R.L., (Eds.). Processes on the Early Earth, p. 133–56, Geological Society of America (GSA), Special Paper 405, GSA, Boulder CO.
Paton, C., Hellstrom, J., Paul, B., Woodhead, J., Hergt, J., 2011. Iolite: freeware for the visualization and processing of mass spectrometer data. J. Anal. At. Spectrom. 26, 2508–2518.
Pyke, J., 2000. Minerals laboratory staff develops new ICP-MS preparation method. AGSO Newsletter 33, 12–14.
Rasmussen, B., Krapez, B., Muhling, J.R., 2014. Hematite replacement of iron-bearing precursor sediments in the 3.46-b.y.-old Marble Bar Chert, Pilbara craton, Australia. Geol. Soc. Am. Bull. 126, 1245–1258.
Rehkamper, M., Halliday, A.N., Fitton, J.G., Lee, D.C., Wieneke, M., Arndt, N.T., 1999. Ir, Ru, Pt and Pd in basalts and komatiites: New constraints for the geochemical behavior of the platinum group elements in the mantle. Geochim. Cosmochim. Acta 63, 3915–3934.
Shapiro, L., Brannock, W.W., 1962. Rapid analysis of silicate, carbonate and phosphate rocks. U.S.G.S., Bulletin 1144-A.
Shukolyukov, A., Kyte, F.T., Lugmair, G.W., Lowe, D.R., Byerly, G.R., 2000. The oldest impact deposits on Earth. In: Koeberl, C., Gilmour, I. (Eds.), Lecture Notes in Earth Science 92: Impacts and the Early Earth. Springer, Berlin, pp. 99–116.
Simonson, B.M., Glass, B.P., 2004. Spherule layers – records of ancient impacts. Ann. Rev. Earth Planet. Sci. 32, 329–361.
Simonson, B.M., Davies, D., Wallace, M., Reeves, S., Hassler, S.W., 1998. Iridium anomaly but no shocked quartz from Late Archaean microkrystite layer: oceanic impact ejecta? Geology 26, 195–198.
Simonson, B.M., Koeberl, C., MacDonald, I., Reimold, W.U., 2000. Geochemical evidence for an impact origin for a Late Archean spherule layer, Transvaal Supergroup, South Africa. Geology 28, 1103–1106.
Simonson, B.M., Cardiff, M., Schubel, K.A., 2001. New evidence that a spherule layer in the late Archean Jeerinah Formation of Western Australia was produced by a major impact. In: 32nd lunar planetary science conference abstracts, lunar and planetary institute contribution 1080, Huston.
Simonson, B.M., Byerly, G.R., Lowe, D.R., 2004. The early Precambrian stratigraphic record of large extraterrestrial impacts. In: Eriksson, P.G., Altermann, W., Nelson, D.R., Catuneau, O., Mueller, W.U. (Eds.), The Precambrian Earth: Tempos and Events. Elsevier, Amsterdam, The Netherlands, pp. 27–45.
Simonson, B.M., Hornstein, M., Hassler, S., 2005. Particles in late archean carawine dolomite (Western Australia) resemble muong nong-type tektites. In: Impacts and the Early Earth, vol. 91, Lecture Notes in Earth Sciences, pp 181–213.
Simonson, B.M., Sumner, D.Y., Beukes, N.J., Johnson, S., Gutzmerd, J., 2009. Correlating multiple Neoarchean-Paleoproterozoic impact spherule layers between South Africa and Western Australia. Precambr. Res. 169, 100–111.
Stefurak, E.J.T., Lowe, D.R., Zentner, D., Fischer, W.W., 2014. Primary silica granules-a new mode of Paleoarchean sedimentation. Geology. http://dx.doi.org/10.1130/G35187.1.

Suganuma, Y., Hamano, Y., Niitsuma, S., Hoashi, M., Hisamitsu, T., Niitsuma, N., Kodama, K., Nedachi, M., 2006. Paleomagnetism of the Marble Bar Chert Member, Western Australia: implications for apparent polar wander path for Pilbara craton during archean time. Earth Planet. Sci. Lett. 252, 360–371.

Sugitani, K., 1992. Geochemical characteristics of Archean cherts and other sedimentary rocks in the Pilbara Block, Western Australia: evidence for Archean seawater enriched in hydrothermally derived iron and silica. Precambr. Res. 57, 21–47.

Terabayashi, M., Masuda, Y., Ozawa, H., 2003. Archean ocean floor metamorphism in the North Pole area, Pilbara Craton, Western Australia. Precambr. Res. 127, 167–180.

Thorpe, R.I., Hickman, A.H., Davis, D.W., Mortensen, J.K., Trendall, A.F., 1990. Application of recent zircon U–Pb geochronology in the Marble Bar region, Pilbara Craton, to modelling Archean lead evolution. In: Glover, J.E., Ho, S.E., (Eds.). Third International Archean Symposium Perth, 1990, Extended Abstracts Volume, Geoconferences (W.A.), Perth, 11–13.

Thorpe, R.I., Hickman, A.H., Davis, D.W., Mortensen, J.K., Trendall, A.F., 1992. U–Pb zircon geochronology of Archean felsic units in the Marble Bar region, Pilbara Craton, Western Australia. Precambr. Res. 56, 169–189.

Trendall, A.F., Compston, W., Nelson, D.R., De Laeter, J.R., Bennett, V.C., 2004. SHRIMP zircon ages constraining the depositional chronology of the Hamersley Group, Western Australia. Aust. J. Earth Sci. 51, 621–644.

Van den Boorn, S.H.J.M., Van Bergen, M.J., Nijman, W., Vroon, P.Z., 2007. Dual role of seawater and hydrothermal fluids in early Archean chert formation: evidence from silicon isotopes. Geology 2007, 939–942.

Van den Boorn, S.H.J.M., Van Bergen, M.J., Vroon, P.Z., De Vries, S.T., Nijman, W., 2010. Silicon isotope and trace element constraints on the origin of ~3.5 Ga cherts: implications for Early Archean marine environments. Geochim. Cosmochim. Acta 74, 1077–1103.

Van Kranendonk, M.J., 2006. Volcanic degassing hydrothermal circulation & the flourishing of early life on Earth: a review of the evidence from c. 3490–3240 Ma rocks of the Pilbara Supergroup Pilbara Craton Western Australia. Earth Sci. Rev. 74, 197–240.

Van Kranendonk, M.J., Hickman, A.H., Williams, I.R., Nijman, W., 2001. Archean geology of the East Pilbara Granite-Greenstone Terrane, Western Australia; a field guide. Geol. Surv. Western Aust. Rec. 9, 134.

Van Kranendonk, M.J., Hickman, A.H., Smithies, R.H., Nelson, D.R., Pike, G., 2002. Geology and tectonic evolution of the Archean North Pilbara Terrain, Pilbara Craton, Western Australia. Econ. Geol. 97, 695–732.

Van Kranendonk, M.J., Smithies, R.H., Hickman, A.H., Champion, D.C., 2007. Paleoarchean development of a continental nucleus: the East Pilbara Terrane of the Pilbara Craton, in Earth's Oldest Rocks. In: Van Kranendonk, M.J., Smithies, R.H., Bennett, V.C. (Eds.), Developments in Precambrian Geology. Elsevier, Amsterdam, The Netherlands, pp. 307–337.

Van Kranendonk, M.J., Smithies, R.H., Griffin, W.L., Huston, D.L., Hickman, A.H., Champion, D.C., Anhaeusser, C.R., Pirajno, F., 2014. Making it thick: a volcanic plateau origin of Paleoarchean continental lithosphere of the Pilbara and Kaapvaal cratons. Geological Society, Special Publications, London, p. 389.

Vernazza, P., Lamy, P., Groussin, O., Hiroi, T., Jorda, L., King, P.L., Izawa, M.R.M., Marchis, F., Biirlan, M., Brunetto, R., 2011. Asteroid (21) Lutetia as a remnant of Earth's precursor planetesimals. Icarus 216, 650–659.

Wingate, M.T.D., Kirkland, C.L., Bodorkos, S., Van Kranendonk, M.J., Hickman, A.H., 2012. 160958: volcaniclastic metasandstone, Trendall Reserve: Geochronology Record 1070. Geological Survey of Western Australia, 6p.